Received: 2 February 2022 | Revised: 2 August 2022 | Accepted: 29 September 2022

DOI: 10.1111/joa.13778

Journal of Anatomy ANATOMICAL SOCIETY WILEY

ORIGINAL ARTICLE

The developing juvenile distal tibia: Radiographic identification of distinct ontogenetic phases and structural trajectories

Rebecca A. G. Reid | **Catriona Davies** | **Craig Cunningham**

Centre for Anatomy and Human Identification, University of Dundee, Dundee, UK

Correspondence
Rebecca A.G. Reid, Centre for Anatomy and Human Identification, University of Dundee, Dundee, UK.
Email: rreid002@dundee.ac.uk

Abstract

A novel combination of radiographic colour gradient mapping and radiographic absorptiometry was utilised to examine 96 human distal tibiae from 54 individuals ranging in age-at-death from the foetal to 23 years. The purpose of this was to identify previously undocumented changes in the internal organisation during the development of the distal tibia and determine whether these changes could be described as distinct phases. Previous studies have demonstrated a rudimentary structural organisation in other skeletal elements that mirror more mature patterns of bone organisation. Results showed that the perinatal tibia did not exhibit a rudimentary structural pattern similar to the architecture observed within the late adolescent tibia. This lack of early internal organisation is hypothesised to be related to the rudimentary ossification process that is being laid down around a pre-existing vascular template which will be subsequently modified by locomotive forces. Between birth and 2 years of age, the tibia exhibited a period of regression where radiodensity decreased in comparison to the perinatal tibia. This period of regression was postulated to be due to a combination of factors including changing locomotive forces, weaning and growth resulting in a stage of development which is extremely demanding on calcium liberation from the skeleton. After 2 years of age, the distal tibia demonstrated refinement where radiographic trajectories progressively developed into patterns consistent with adult trabecular organisation. These trajectories are linked to the forces associated with the bipedal gait, suggesting a strong influence of biomechanical forces on the development of the distal tibia.

KEYWORDS
biomechanics, development, juvenile, radiography, Tibia

1 | INTRODUCTION

The development of the juvenile skeleton is a dynamic process during which bone must increase in size while also changing in shape and structure to accommodate the stresses that are placed upon it. In the adult skeleton, bone functional adaptation and the Mechanostat Hypothesis describe how bone adapts to stresses imposed upon the skeleton (Frost, 2003; Ruff et al., 2006). In particular, the trabecular architecture of bone has been demonstrated to remodel to accommodate stresses imposed upon the skeleton (Barak et al., 2011;

Currey, 1984; Ruimerman et al., 2005). Nonmechanical factors, such as hormones and growth factors, also act to guide this mechanism, as does the regulation by epigenetic, extragenetic and genetic influences (Frost, 1998; Skedros et al., 2007). There is a growing understanding of how the juvenile skeleton responds to changing forces, however, this remains an area of active research with gaps within the knowledge remaining (Ryan et al., 2017; Saers et al., 2022).

The advancements of imaging technologies have allowed for expansion of research into the development of juvenile trabecular bone, progressing from destructive traditional histological techniques to non-destructive, higher resolution microcomputed tomography (μCT) studies. Long bones comprise the majority of the research previously studied, including the femur (Djuric et al., 2012; Milovanovic et al., 2017; Modlesky et al., 2014; Osborne et al., 1980; Reissis & Abel, 2012; Ryan et al., 2017; Ryan & Krovitz, 2006; Salle et al., 2002), tibia (Burrows et al., 2010; Ding et al., 2012; Goliath et al., 2022; Gosman & Ketcham, 2009; Raichlen et al., 2015), humerus (Perchalski et al., 2018; Reissis & Abel, 2012; Ryan et al., 2017) and radius (Colombo et al., 2019). However, there is a growing interest in the development of irregular bones such as the ribs (Beresheim et al., 2020), vertebral column (Acquaah et al., 2015; Goodchild, 2019; Kneissel et al., 1997; Nuzzo et al., 2003; Roschger et al., 2001; Yusof, 2013), innominate (Abel & Macho, 2011; Cunningham & Black, 2009a, 2009b; Glorieux et al., 2000; Maclean, 2017; Maclean et al., 2014), scapula (O'Malley, 2013) and calcaneus (Saers et al., 2019).

Currently, the distal tibia has only been examined in individuals aged 1.3–8.5 years by Raichlen et al. (2015) and those between 15 and 20 years by Burrows et al. (2010). Raichlen et al. (2015) observed a correlation with locomotion and degree of anisotropy (DA), the extent to which trabeculae are similarly aligned. DA displayed more inter-individual variation at younger ages, with some individuals displaying an isotropic organisation, while others had an anisotropic organisation. This occurred when the ankle is less stable due to the learning process of walking and development of the bipedal gait. When bipedal gait fully developed, the ankle exhibited greater stability which was hypothesised to result in the lower variation in DA observed between individuals, with individuals displaying higher mean DA. The authors suggest that the organisation of the trabeculae at younger ages accommodates the disorganised loading patterns attributed to the acquisition of walking.

Burrows et al. (2010) examined the distal tibia using high resolution peripheral quantitative computer tomography (HR-pQCT) in a sample of 279 living individuals aged 15–20 years. The authors examined a section of the distal tibia proximal to the tibial plafond. No significant changes in trabecular bone volume fraction (BV/TV), the ratio of trabecular bone volume to total volume of interest and trabecular density were observed between the ages studied, suggesting that the distal tibia trabecular bone is characteristically mature after 15 years of age. Notably, however, male BV/TV, trabecular density, number of trabeculae (Tb.N), and cortical thickness demonstrated significantly higher values than in females, suggesting that sexual dimorphism is present in trabecular bone following puberty. The lack of examination of the distal tibia in foetal and perinatal specimens, and individuals between 9 and 14 years demonstrates the need for this research as this bone has an important role in locomotion and weight-bearing within the ankle joint.

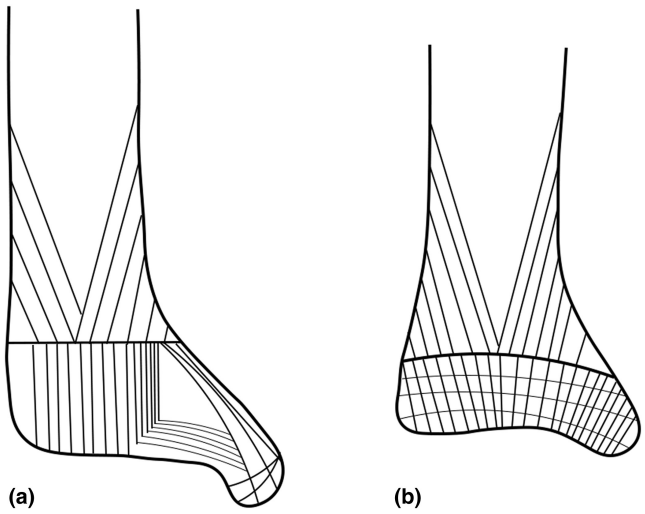

FIGURE 1 Schematic of the trabecular organisation within the distal tibia. Black lines represent trabecular bundles. (a) Frontal plane; (b) sagittal plane. Reproduced from Takechi et al. (1982).

Bodyweight is transmitted from the head through the thorax and vertebral column to the pelvis, through the lower limbs and into the foot via the ankle joint during bipedal gait and passive standing (Soames & Palastanga, 2019). The distal articular surface of the adult tibia has been described as containing thick vertically aligned trabeculae (Figure 1; Takechi et al., 1982), where high BV/TV values have also been reported (Tsegai et al., 2017). It is likely these trabeculae are adapted to facilitate the transmission of high compressive loads through to the talus (Procter & Paul, 1982; Stauffer et al., 1977). Du et al. (2019) and Sode et al. (2010) observed high BV/TV values in the medial and posterior regions of the adult distal tibia and attributed this to large compressive and shearing forces applied in these areas. Takechi et al. (1982) and Tillmann et al. (1985) also describe the trabeculae within the medial malleolus and proposed its structure to be aligned to compressive forces in addition to facilitating tensile forces caused by collateral ankle ligaments (Figure 1). The internal structure of the distal tibia appears to be strongly linked to its biomechanical function. However, the reaction of the juvenile distal tibia to the changing biomechanical forces is not yet fully understood, in particular, its response to the forces associated with the acquisition of different motor milestones during development such as sitting upright, crawling and walking.

Previous research has demonstrated distinct changes that occur within the trabecular skeleton during specific age ranges. There is a substantial increase in trabecular volume during the gestational period, described by Acquaah et al. (2015) as 'gestational overproduction'. This is hypothesised to be in preparation for the subsequent bone modelling and remodelling occurring after birth. Also, within the foetal skeleton, rudimentary patterns consistent with adult form have been identified in the ilium (Abel & Macho, 2011;

Cunningham & Black, 2009a, 2009b), the sacrum (Yusof, 2013), and the scapula (O'Malley, 2013), however, this has not been observed within long bones (Gosman & Ketcham, 2009; Raichlen et al., 2015; Ryan & Krovitz, 2006). The occurrence of these rudimentary patterns has been hypothesised to be a result of a pre-determined genetic template, vascularisation and/or intrauterine movements (Cunningham & Black, 2009a, 2009b, 2010, 2013). As a result of gestational overproduction, during the perinatal period, high BV/TV values have been observed throughout the skeleton (Acquaah et al., 2015; Beresheim et al., 2020; Colombo et al., 2019; Gosman & Ketcham, 2009; Milovanovic et al., 2017; Ryan et al., 2017; Ryan & Krovitz, 2006; Saers et al., 2019). At this stage, the trabecular architecture of bones has been described as typically dense and isotropic with numerous thin trabeculae which may be associated with gestational overproduction (Djuric et al., 2012; Gosman & Ketcham, 2009; Saers et al., 2019).

During the first year of life, there is a distinct decrease in trabecular quantity and reorganisation in architecture, labelled as a period of 'constructive regression' (Acquaah et al., 2015). At approximately 6 months of age, a decrease in BV/TV has been observed in the femur (Milovanovic et al., 2017; Ryan et al., 2017; Ryan & Krovitz, 2006), tibia (Gosman & Ketcham, 2009), calcaneus (Saers et al., 2019), humerus (Ryan et al., 2017), vertebrae (Acquaah et al., 2015) and ischium (Maclean, 2017). This has been attributed to lack of biomechanical influences occurring between birth and the onset of walking which results in a resorption of bone (Saers et al., 2019). This decrease in trabecular quantity has also been postulated to be a result of weaning which occurs at approximately 6 months of age, with a decrease in dietary calcium demanding an increase in calcium liberation from the skeleton (Moore et al., 2014). However, the previous research which has identified a 'constructive regression' period, has largely pertained to Medieval skeletal collections, with the exception of Acquaah et al. (2015) who examined a 19th century British population and Maclean (2017) who examined the Scheuer Collection. Therefore, weaning at 6 months is unlikely to occur in these archaeological populations, and other factors driving the regression need to be considered. The infant growth spurt also results in a great physiological demand for calcium liberation from the skeleton (Lejarraga, 2012) and is also proposed to influence this regressive period. After 1 year of age, trabecular bone throughout the skeleton has been observed to go through a period of 'refinement' (Acquaah et al., 2015), becoming structurally organised to withstand bipedal forces and typically acquires an adult form by 8 years of age as observed in the tibia (Gosman & Ketcham, 2009), calcaneus (Saers et al., 2019) and vertebrae (Roschger et al., 2001). Further to this, factors such as vascularisation and metaphyseal location have been observed to influence the structural heterogeneity of the trabecular and cortical skeleton (Byers et al., 2000; Cunningham & Black, 2009c; Fazzalari et al., 1997; Modlesky et al., 2014; Salle et al., 2002).

The patterns in the development of the juvenile skeleton have emerged with expanding research. The distinct changes that occur within the skeleton not only seem to be influenced by changing biomechanical forces during development but also appear to have non-mechanical regulation. The precise relationships and interactions between these genetic and epigenetic factors upon the development of the skeleton, however, are still not completely understood. Additionally, why adult trabecular organisation is prevalent within the prenatal scapula, ilium and sacrum (Abel & Macho, 2011; Cunningham & Black, 2009a, 2009b; O'Malley, 2013; Yusof, 2013) but not others such the prenatal femur (Salle et al., 2002) is unknown. The examination of the trabecular development of the complete skeleton throughout ontogeny has not been examined, and as a result, the influence of factors such as different ossification and vascularisation patterns is not fully understood (Cunningham & Black, 2013). By combining an understanding of the changing biomechanical influences on the skeleton during ontogeny and the anatomy of the ankle joint with an investigation of the internal structure of the distal tibia, this study aims to contribute to the growing understanding of the developing juvenile skeleton. Analysis of the developing skeleton may have important clinical applications, in the treatment of paediatric trauma and therapeutic intervention of some pathological conditions, such as juvenile idiopathic arthritis of the ankle joint.

Preliminary radiographic studies have been previously adopted in investigations of juvenile skeletal development (Cunningham & Black, 2009a; Goodchild, 2019; Maclean, 2017; Maclean et al., 2014; O'Malley, 2013; Yusof, 2013). Radiographic colour maps have been established to be a useful tool for ontogenetic analysis by radiographic results from Cunningham and Black (2009a) and Maclean et al. (2014) demonstrating consistent findings with subsequent microcomputed tomography results from Cunningham and Black (2009b) and Maclean (2017). While microcomputed tomography studies provide more information than radiographic examinations, in particular the three-dimensional quantification of bone microstructure, radiographic inspection of the juvenile ankle remains important for clinical assessment of paediatric injuries due to its accessibility, quick acquisition and low costs (Marsh & Daigneault, 2000; Reed & Black, 2010).

Within prior research utilising radiography to examine skeletal development, colour gradient maps were created in Adobe Photoshop by converting grey levels from radiographs to a corresponding colour based on radiopacity (Cunningham & Black, 2009a; Goodchild, 2019; Maclean, 2017; Maclean et al., 2014; O'Malley, 2013; Yusof, 2013). For 8-bit radiographic images, 256 grey levels exist, ranging from 0 to 255. Areas of high bone intensity were illustrated by a specific colour while areas of low bone intensity were demarcated by another colour. Notably, these colours were attributed to different bone intensities, not bone densities due to a lack of calibration phantom. The presence of an aluminium step wedge presents an opportunity to correlate grey level values to a measure of relative bone density, using methods adopted within radiographic absorptiometry (Bowen et al., 2013; Hirvasniemi et al., 2019; Ilić et al., 2020; Nackaerts et al., 2007; Sun et al., 2008; van Rijn et al., 2000).

Radiographic absorptiometry is a technique utilised for quantification of bone density within dental (Nackaerts et al., 2007; Sun

et al., 2008) and veterinary examinations (Bowen et al., 2013; Ilić et al., 2020). It has also been examined as a clinical screening tool for assessing bone density in human patients to identify those with osteoporotic risk (Gasser et al., 2005). Therefore, radiographic absorptiometry serves as an accessible, standardised preliminary investigative analysis of internal bone structure.

The underlying principle of radiographic absorptiometry is the presence of a step wedge to calibrate levels of x-ray absorption (Trouerbach, 1982). Typically, aluminium step wedges are utilised for osseous studies, as the absorption and scatter properties of aluminium are similar to those of bone (Trouerbach, 1982). Specific regions of interest within bone can therefore be compared to a reference step wedge and expressed as a measure of relative bone mineral density. Therefore, this study introduces a novel method which combines colour gradient maps with quantitative radiographic absorptiometry to standardise the radiographs.

2 | MATERIALS AND METHODS

2.1 | Sample selection

The distal aspect of 96 human tibiae from 54 individuals were examined from the Scheuer Collection which is housed within the Centre for Anatomy and Human Identification, University of Dundee. The Scheuer Collection is an active juvenile skeletal repository from European archaeological and historical anatomical sources. Documented information was available for 13 individuals, with age-at-death being estimated for most of the sample. Three historical anatomical specimens were included in this study, with the remainder being archaeological. Ethical approval is in place for research upon this skeletal collection from the HM Inspector for Anatomy, Scotland. Specimens included in this analysis ranged from 28 intrauterine weeks to 23 years of age (Table 1). Specimens were selected based on the following criteria: no extensive post-mortem damage, pathology or soft tissue, nor articulated with other skeletal elements. Specimens with minimal post-mortem damage, were included in the sample as given the nature of archaeological populations, it is extremely difficult to avoid post-mortem damage. The specimens with post-mortem damage exhibited cortical erosion and if damage to the trabecular was present, it was deemed minimal.

2.2 | Radiography

Specimens were radiographed within the Centre for Anatomy and Human Identification, University of Dundee using a Saxo Mobile X-ray Unit. Exposure settings of 55 kV and 1.6 mA, with a focal distance of 100 cm were utilised throughout the radiographic study. The anteroposterior (AP) and lateral views of the tibia were radiographed, following a preliminary study to select the most suitable radiographic views which minimised tissue superimposition. If present, but unfused, the distal tibial epiphysis was manually re-articulated without an adhesive medium to the distal metaphysis. An Artinis Step Wedge Type 3 was placed in each radiograph. This step wedge consists of 96% aluminium with five steps of 2.5 mm, 3.5 mm, 4.75 mm, 7 mm and 9 mm thickness. Resultant radiographic images were saved as a JPG file for subsequent colour mapping and analysis.

2.3 | Radiographic absorptiometry and colour mapping

Radiographic images were opened in Adobe Photoshop 2021 version 22.3.1 to measure grey values and produce colour gradient maps. An area consisting of approximately 26mm^2 (3600 pixel^2) within each step of the step wedge included in each image was selected using the freeform 'rectangular' selection tool. Additionally, 26mm^2 (3600 pixels^2) of the radiograph background was selected to represent 0 mm on the step wedge. Mean grey level was measured in these areas using the histogram tool in Adobe Photoshop.

Calibration plots of aluminium bone mineral density equivalents (Al BMDEs) versus grey levels were produced for each individual image. Al BMDE for each step on the step wedge was calculated by multiplying the known step thickness by the known step wedge density. The resultant Al BMDE values were then plotted against the measured mean grey value for each step on the step wedge. A third-order polynomial trendline was then added for each plot. The

TABLE 1 Sample composition

Age		Number of specimens	Number of individuals	Left	Right
Foetal	28–38 weeks	5	3	2	3
Perinatal	Birth	34	17	17	17
Infancy	0 – ≤12 months	8	5	5	3
Early Childhood	>12 months– ≤8 years	19	12	9	10
Late Childhood	>8 years	30	17	16	14
Total		96	54	49	47

Note: Definitions of early and late childhood adapted from Ryan et al. (2017) who divided childhood into early; 1–5 years, middle; 5–10 years and late; 10–18 years. In this study, childhood was subdivided into two periods before and after 8 years of age due to the observations throughout the literature that typically, adult trabeculae quantity and structure are achieved at 8 years of age, as observed in the tibia (Gosman & Ketcham, 2009), calcaneus (Saers et al., 2019) and vertebrae (Roschger et al., 2001).

equation and statistics for each plot were calculated using the 'linest' function in Microsoft Excel.

The 'gradient editor' tool within Adobe Photoshop was used to produce colour maps following a protocol documented in previous studies (Cunningham & Black, 2009a; Maclean et al., 2014). Four colours (yellow, violet, orange and blue) were applied to the colour gradient. Yellow was utilised as a baseline and the yellow 'stop' was placed at an appropriate location on the gradient so that the background of the radiograph was a solid yellow colour. The remaining colours were then distributed equally throughout the rest of the greyscale spectrum. The transition between each colour was placed equally between 'stops'. The resulting colour gradient therefore divides the greyscale spectrum into four colours that are each a specified range of grey levels.

The AI BMDE of each colour was then calculated using the calibration plot produced for each image. The percentage location of each 'stop' along the grey level spectrum was used to calculate the associated grey value for that location. These known grey values were entered into the third-order polynomial equation produced for each image to calculate the AI BMDE value for each stop. An AI BMDE scale bar was then produced for each image.

2.4 | Developmental analysis

The colour maps for all individuals were placed in groups of shared morphology and radiographic patterns, such as the consistent development of the epiphysis and shape of the diaphysis, without any knowledge of age-at-death of the specimens. Age-at-death information was added to each group once all the colour maps had been assigned to a group. Areas of violet were interpreted as areas of low AI BMDE values, orange as medium AI BMDE values and blue as areas of high AI BMDE values.

2.5 | Intraobserver and interobserver agreement analysis

To assess intraobserver agreement and bilateral asymmetry, each colour map was anonymised and re-assigned to a development group, without knowledge of which individual each specimen belonged to, or age-at-death. This was conducted 12 months after the original analysis. The developmental group assigned was compared to the original assessment using a weighted kappa analysis with linear weights (Cicchetti & Allison, 1971) to assess agreement. Bilateral asymmetry was assessed by comparing if each tibia had been assigned to the same developmental group as its antimere.

Interobserver agreement was assessed by a second observer with comparable experience of radiographic osteological analysis. The observer was asked to assign each colour map to a developmental group based on the descriptions of each group provided by the original analyst. Observer 2 had no knowledge of age-at-death or which individual each specimen belonged to. The developmental group assigned was compared between observed using weighted kappa analysis with linear weights (Cicchetti & Allison, 1971) to assess agreement. Statistical analysis was conducted using SPSS v28. Ethical approval was granted by the University of Dundee's School of Science and Engineering Ethics Committee.

3 | RESULTS

Colour maps of the distal tibia were divided into seven development groups (Table 2; Figure 2) based on a shared morphology and radiographic patterns (Figures 3 and 4). Due to this, overlapping age rages between developmental groups were observed (Figure 2).

3.1 | Intraobserver and interobserver agreement results

To assess intraobserver agreement, the placement of colour maps of 96 specimens into developmental groups was repeated 12 months after the original analysis. There was a statistically significant agreement between the two analyses, $\kappa_w = 0.986$ (95% CI, 0.970 to 1.002), $p < 0.0005$. The strength of agreement was classified as very good according to Landis and Koch (1977). A second observer also assigned each colour map to a developmental group based on the descriptions of each group provided by the original analyst. There was a statistically significant agreement between the two observers, $\kappa_w = 0.828$ (95% CI, 0.772 to 0.885), $p < 0.0005$. The strength of agreement was classified as good to very good according to Landis and Koch (1977).

3.2 | Bilateral asymmetry

Development of the tibiae was assessed to be consistent between right and left specimens. Out of 54 individuals, only three individuals (0.06%) had pairs of tibiae which were assigned to differing development groups. When this occurred, these were individuals that were assigned as either least or most mature of each group and each tibia were classified into neighbouring developmental groups.

TABLE 2 Developmental groups

Group	Number of specimens	Number of individuals	Age range
1	5	3	Foetal
2	34	17	Birth–6 months
3	9	6	Birth–2 years
4	14	9	2–10 years
5	8	4	7–9 years
6	11	6	10–14 years
7	15	9	16–23 years

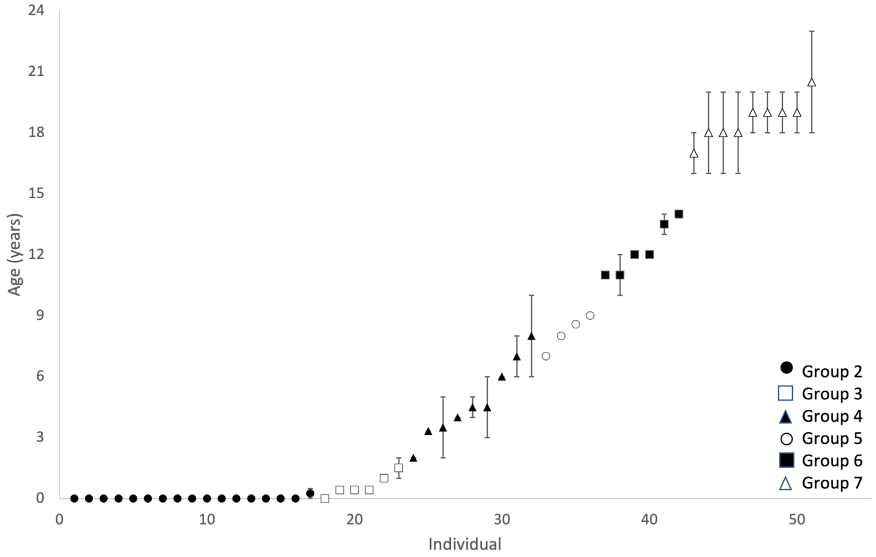

FIGURE 2 Age distribution of each developmental group, excluding Group 1. Most individuals had an estimated age-at-death range, while 13 individuals had a documented age-at-death. Perinatal individuals were assigned as 0 years of age.

3.2.1 | Group 1 (Foetal)

Within this group of three individuals (n = 5 tibiae), the distal tibia flared medially with a flat metaphyseal surface that appeared square-like with rounded edges and lacked prominent osteological features. Due to the small size of these specimens, radiographic details were limited, however, a shared pattern was observed between specimens of this group (Figures 3 and 4). Radiolucency of the distal-most portion of the tibia was observed, associated with low AI BMDE (Figure 5, arrows 2,3, and 5).

3.2.2 | Group 2 (Birth–6 months)

In comparison to specimens assigned to Group 1, Group 2 specimens, comprising of 17 individuals (n = 34 tibiae), demonstrated an increase in AI BMDE depicted by the presence of violet and orange within the colour maps (Figures 3 and 4). A pattern was observed from the AP view, appearing as orange struts radiating inferiorly from between the central and medial margin of the midshaft into the distal end of the tibia, and increasing in prevalence with proximity to the distal end of the bone (Figure 6, arrows 2 and 3). This was typically demarcated by an orange colour indicating values of medium AI BMDE throughout. From the lateral view, an orange triangular-shaped area of elevated AI BMDE was observed in several specimens with the superior apex of the triangle extending from the anterior surface of the bone and into the distal end of the bone (Figure 6, arrow 5).

3.2.3 | Group 3 (Birth–2 years)

The six individuals (n = 9 tibiae) assigned to Group 3 were radiographically distinct from the rest of the tibiae sample due to their considerable radiolucency (Figures 3 and 4). The radiolucency was demonstrated by the observable yellow background through the violet bone structure (Figure 7, arrows 2 and 5). This radiolucency observed within the distal tibia is suggestive of a decrease in AI BMDE in comparison to Group 2 perinatal specimens (Figures 3 and 4). Due to the radiolucency at this stage, radiographic features are limited, although the anterior, posterior, medial, lateral and distal margins of the bone appear well-defined in comparison to the low central radiopacity (Figure 7, arrows 1,3, and 4).

3.2.4 | Group 4 (2–10 years)

After 2 years of age, an increasingly distinct pattern of developing internal bone organisation was observed (Figures 3 and 4). Group 4, consisting of nine individuals (n = 14 tibiae), featured a general increase in radiodensity in comparison to Group 3, indicating an increase in AI BMDE at approximately 2 years of age (Figures 3 and 4). Linear trajectories were observed in these specimens extending inferiorly from the anterior, medial, lateral and posterior margins of the bone and into the distal-most region of the bone where this pattern appeared to converge in a mesh-like network (Figure 8, arrows 2, 4–6,8,9). This convergence typically was demarcated by orange and blue indicating an area of medium to high AI BMDE (Figure 8, arrows 5, 9). The trajectories were observable by their contrast in colour from their background, for example they typically appeared orange against a violet background.

3.2.5 | Group 5 (7–9 years)

This group of four individuals (n = 8 tibiae) exhibited development of the radiographic patterns observed within Group 4, with the trajectories more pronounced in this group (Figures 3 and 4). The trajectories descending from the anterior, medial, lateral and posterior

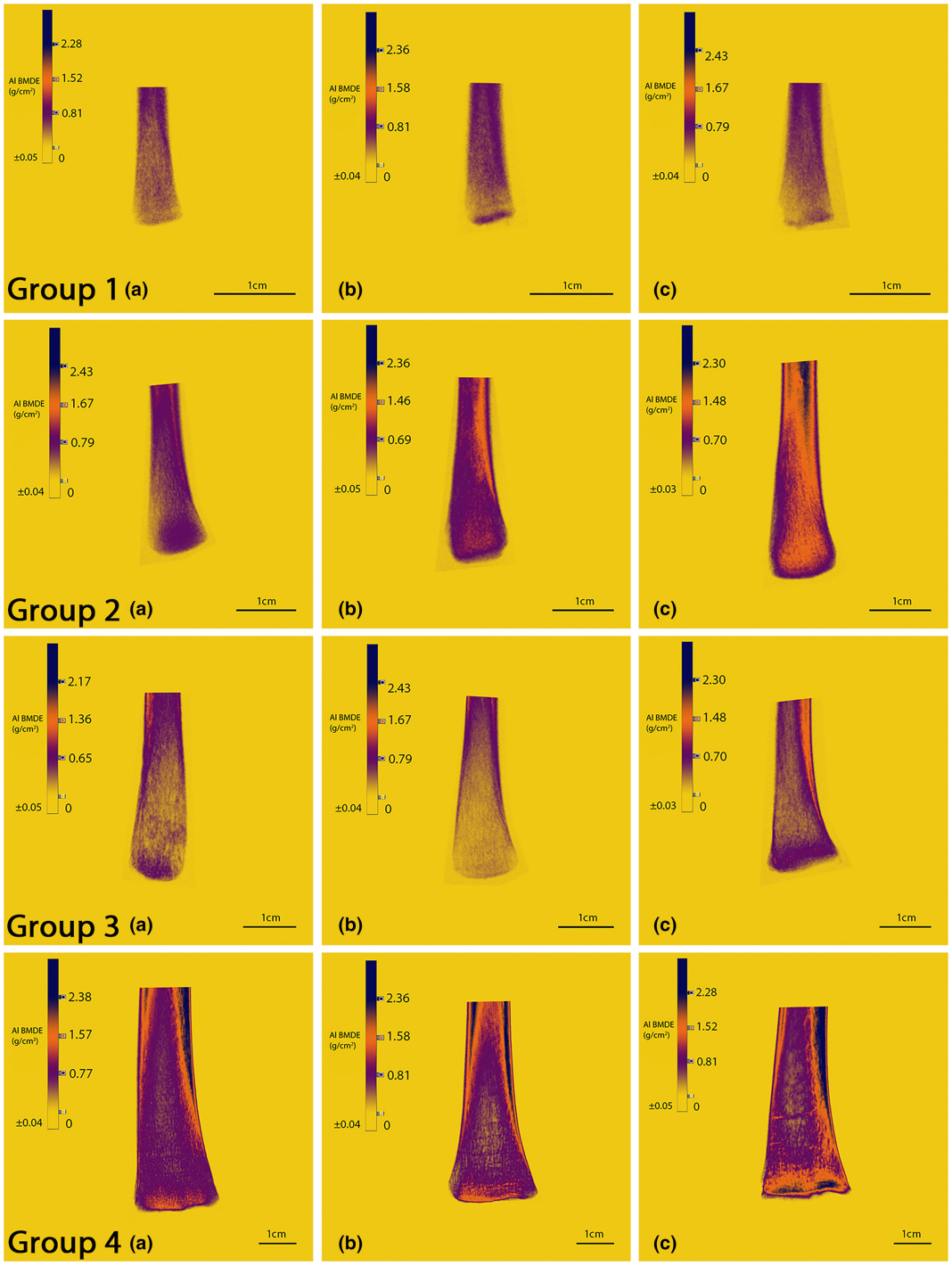

FIGURE 3 Anteroposterior view of the developing distal tibia. Most tibiae illustrated are right sided. (a) Least developed; (b) median development; (c) most developed specimen within each developmental group. AI BMDE scale in each image.

margins of the bone appeared as distinct orange rays of medium AI BMDE (Figure 9, arrows 1 and 5) and converged into the distal-most aspect of the tibia appearing as a solid orange or blue colour indicating medium to high AI BMDE (Figure 9, arrows 2 and 6).

In the distal epiphysis, vertical trajectories were observed between superior and inferior margins of the epiphysis (Figure 9, arrows 4 and 8). The superior and inferior margins of the distal epiphysis tended to have higher AI BMDE values than the centre of the epiphysis (Figure 9, arrow 7). The developing medial malleolus exhibited reduced radiodensity indicating low AI BMDE (Figure 9, arrow 3). Within this region, a trajectory was observed fanning infero-medially from the supero-lateral aspect of the medial malleolus (Figure 9, arrow 3).

3.2.6 | Group 6 (10–14 years)

Group 6 consisted of six individuals ($n = 11$ tibiae) with greater development of the distal epiphysis in comparison to Group 5, however,

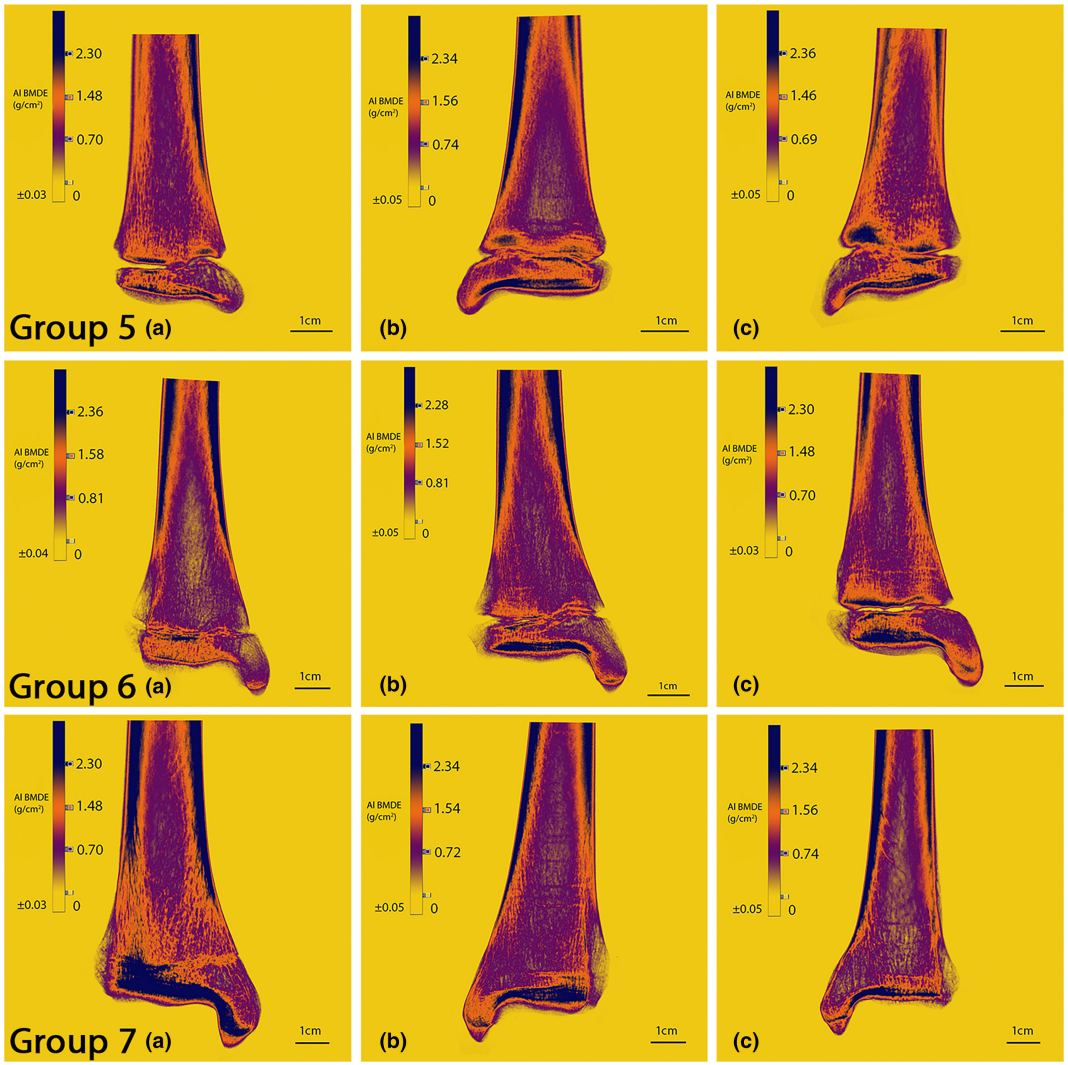

FIGURE 3 (Continued)

still lacked distal epiphyseal fusion (Figures 3 and 4). However, bone bridging, the vertical extensions of bone between the epiphysis and metaphysis (White et al., 2008), was apparent between the distal metaphyseal surface and the epiphysis. The tibial diaphysis shared radiographic patterns with those identified in Group 5, with trajectories extending inferiorly from the medial, lateral, anterior, and posterior margins of the bone to converge in the distal-most aspect of the tibia (Figure 10, arrows 1, 2, 6 and 7).

The distinguishing feature of Group 6, in comparison to Group 5, was the development of the medial malleolus which had increased in volume with the colliculi becoming defined. As with Group 5, vertical trajectories were observed between areas of high AI BMDE located in the superior and inferior margins of the epiphysis (Figure 10, arrows 3 and 8). In the medial malleolus, the superior aspect displayed reduced radiodensity, indicated by the visible yellow background through the violet bone structure, in comparison to the more solid violet in the remainder of the malleolus, indicating low AI BMDE (Figure 10, arrow 4). Within this region, a trajectory was observed fanning out inferomedially from the superior-lateral aspect of the medial malleolus (Figure 10, arrow 4). The lateral view allowed greater radiographic detail of the medial malleolus. From this view, a triangular radiolucency was observed within the centre of the medial malleolus (Figure 10, arrow 10). Meanwhile, fine linear trajectories of low AI BMDE were observed extending inferiorly from the superior aspect of the anterior and posterior colliculi towards intercollicular groove (Figure 10, arrow 11). Within the intercollicular groove, an orange arch-shaped region of increased radiodensity was observed (Figure 10, arrow 12).

3.2.7 | Group 7 (16–23 years)

The distal tibial epiphyses of the nine individuals (n = 15 tibiae) assigned to this group exhibited partial to complete fusion. Trajectories were observed extending inferiorly from the medial, lateral, anterior and posterior margins of the bone to converge in the most distal portion of the tibia (Figure 11, arrows 1, 7 and 8). These trajectories were typically orange toward the margins of the bone and violet within the shaft. In individuals with partial epiphyseal union, these

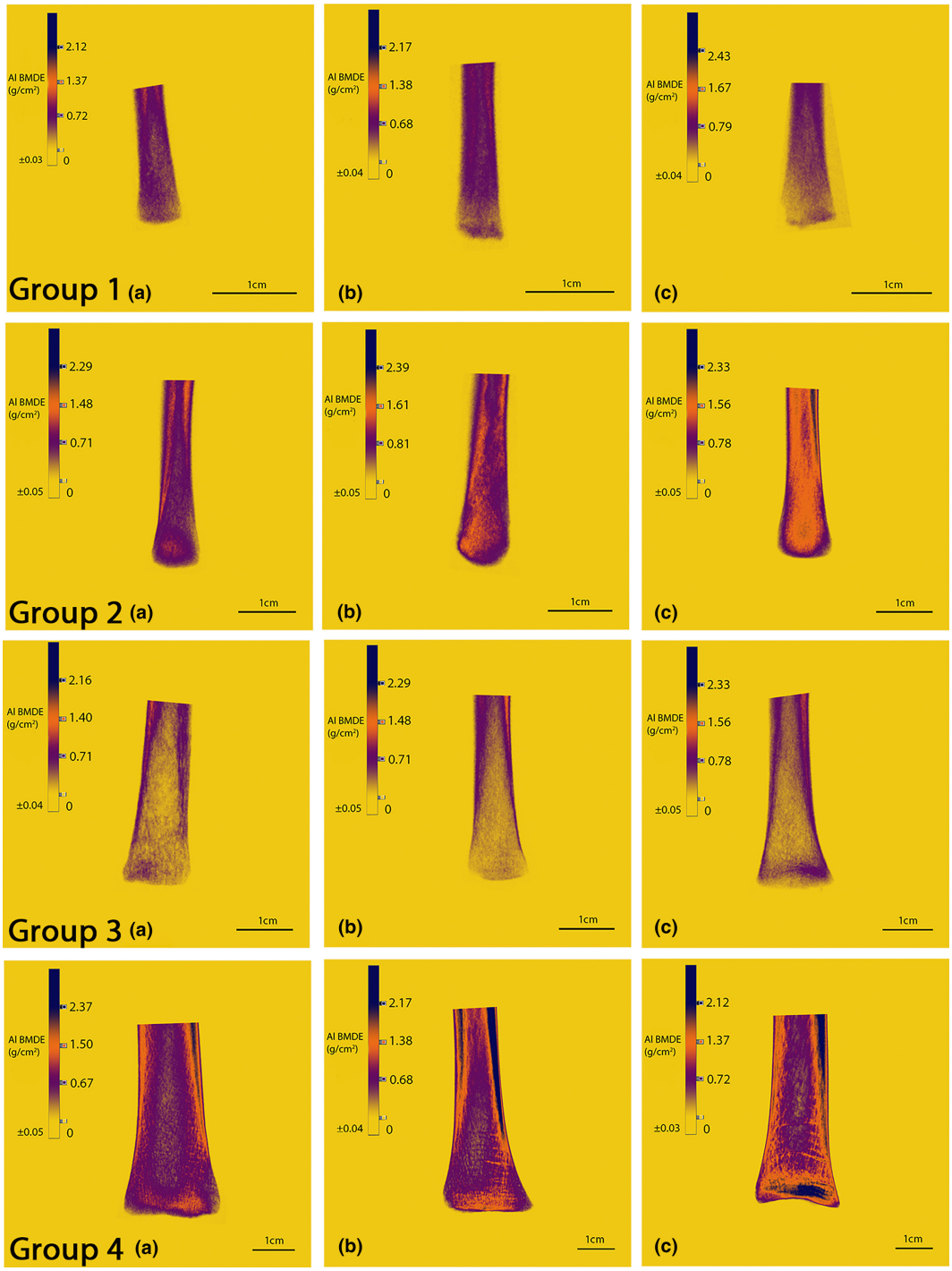

FIGURE 4 Lateral view of the developing distal tibia. Most tibiae illustrated are right sided. (a) Least developed; (b) median development; (c) most developed specimen within each developmental group. AI BMDE scale in each image.

trajectories appeared to end at, or be interrupted, by the epiphyseal line, however, in individuals with complete fusion, these trajectories extended completely to the distal margin of the bone (Figure 11, arrows 2, 4, 5, and 9). Radiodensity of the epiphyseal line decreased with increasing fusion, as demonstrated by the reduction in blue demarcating the line indicating decreased AI BMDE (Figure 11, arrows 2, 5, and 9). The medial malleolus demonstrated shared trajectories with Group 6 (Figures 3 and 4). Meanwhile, in all specimens, the region immediately superior to the distal articular surface exhibited high AI BMDE demarcated by blue (Figure 11, arrows 6 and 10).

4 | DISCUSSION

The developing tibia demonstrated distinct ontogenetic phases. The development of the distal tibia can therefore be subdivided

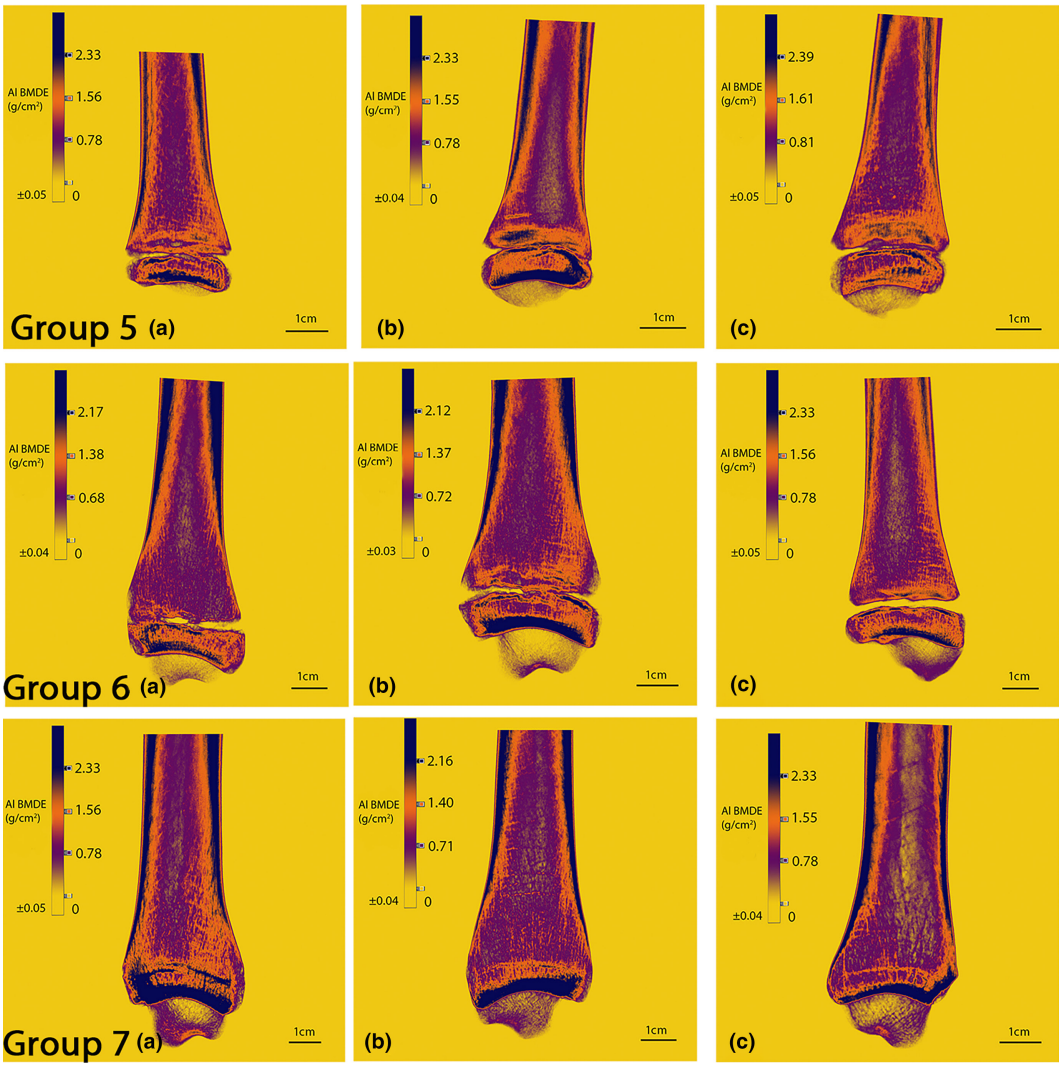

FIGURE 4 (Continued)

into different phases; foetal, perinatal, regression (0–2 years) and refinement (>2 years), which agrees with the progression of ontogeny described within other regions of the skeleton (Acquaah et al., 2015; Beresheim et al., 2020; Colombo et al., 2019; Gosman & Ketcham, 2009; Maclean, 2017; Milovanovic et al., 2017; O'Malley, 2013; Ryan et al., 2017; Ryan & Krovitz, 2006; Saers et al., 2019).

4.1 | The foetal tibia

The small size of the foetal specimens limited radiographic detail of these bones. Radiographically, the tibia appeared consistent with previously reported patterns of ossification beginning at the midshaft, progressing towards the distal and proximal ends of the bone (Baumgart et al., 2019). The radiolucency observed at the distal end of the tibia, in comparison to towards the midshaft, was likely attributed to the lack of ossification, rather than size differences. Taphonomic condition of each bone was documented prior to radiography and considered while making radiographic observations, thus was unlikely to result in this radiolucency.

4.2 | The perinatal tibia

The perinatal distal tibia did not demonstrate radiographic patterns similar to the mature tibia as has been observed in other bones (Cunningham & Black, 2009a). This mature structure consists of trajectories descending from the medial, lateral, anterior and posterior boundaries of the diaphysis inferiorly and obliquely towards the centre of the distal surface of the bone (Figure 1). Instead, in the perinatal tibia, a trajectory appeared to descend more centrally and 'fan' out to the distal end of the bone (Figure 6). Rudimentary prenatal patterns consistent with adult structure have previously been observed in the ilium (Abel & Macho, 2011; Cunningham & Black, 2009a, 2009b), sacrum (Yusof, 2013) and scapula (O'Malley, 2013) but not within long bones (Gosman & Ketcham, 2009; Raichlen et al., 2015; Ryan & Krovitz, 2006). The

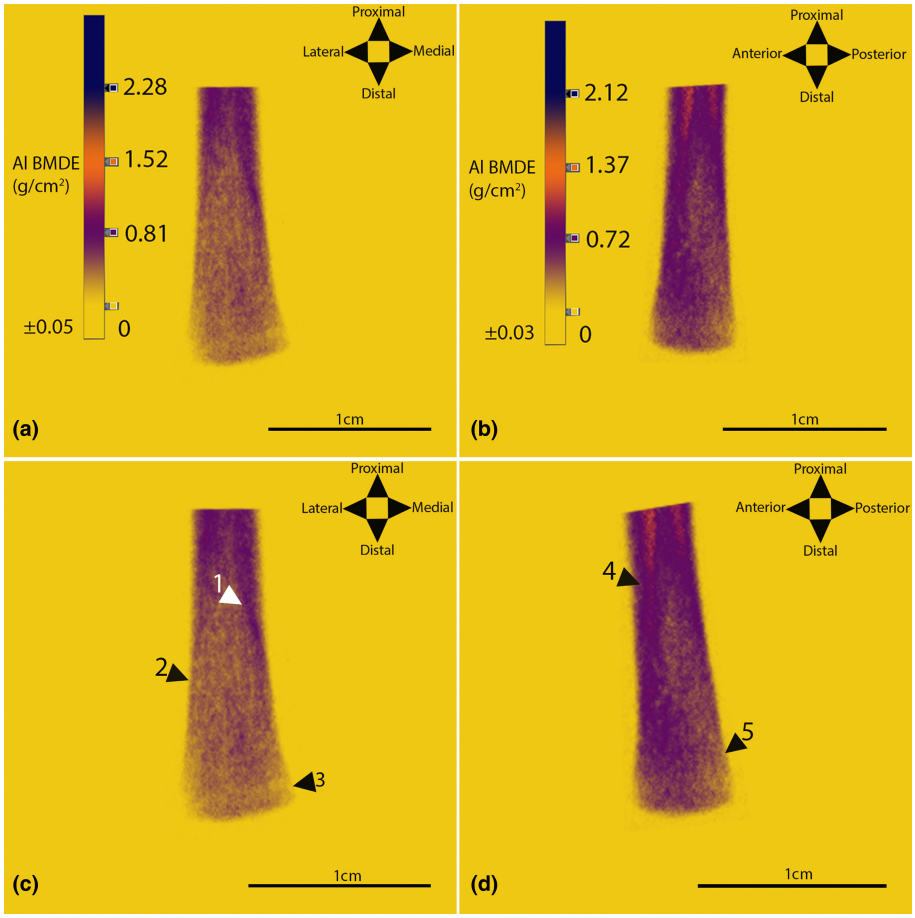

FIGURE 5 Annotated example of a colour gradient map of the right distal tibia from a Group 1 individual. (a, c) Anteroposterior view; (b, d) lateral view. Arrow descriptions are contained within Table 3.

TABLE 3 Radiographic features of a Group 1 tibia

Arrow	Feature
1	The medial and lateral portions of the midshaft appear dark violet, indicating low AI BMDE
2	The distal portion of the bone is comprised of lower AI BMDE than the areas highlighted by arrow 1, due to differing shades of violet
3	Area of radiolucency parallel to the distal articular surface of the tibia, associated with low AI BMDE
4	Orange line indicating medium AI BMDE extending down the anterior aspect of the tibial midshaft. The rest of the midshaft and anterior aspect appears dark violet
5	The posterior distal half of the tibia and entire distal-most aspect appears a light violet colour, indicating a lower AI BMDE than the areas highlighted by arrow 4

Note: Arrows pertain to Figure 5.

lack of organisation within the perinatal distal tibia and other long bones in comparison to the ilium, may be a result of the difference in vascularisation patterns. In an investigation of the neonatal ilium, a vascular collar of cortical bone extending into the trabecular bone was observed originating from the nutrient foramen (Cunningham & Black, 2013). Thickened trabeculae were observed surrounding this collar. The nutrient foramen provides blood to the bone via the nutrient artery and its invasion triggers endochondral ossification. As a result, the presence of the nutrient artery precedes the formation of trabeculae which must therefore grow around the vessels, which thus influence the trabecular architecture (Cunningham & Black, 2013). This pattern of thickened trabeculae around vasculature has also been observed within the scapula and ischium (Maclean, 2017; O'Malley, 2013). Therefore, the presence of vessels likely results in areas of radiolucency where the bone must allow space for the invading vasculature. While the ilium experiences a complex vascular pattern that originates from several branches of arteries (Cunningham & Black, 2010), the tibial vascularisation is simpler. At the end of the embryonic period, vascular invasion is evident in the prenatal tibial diaphysis (Cunningham et al., 2016;

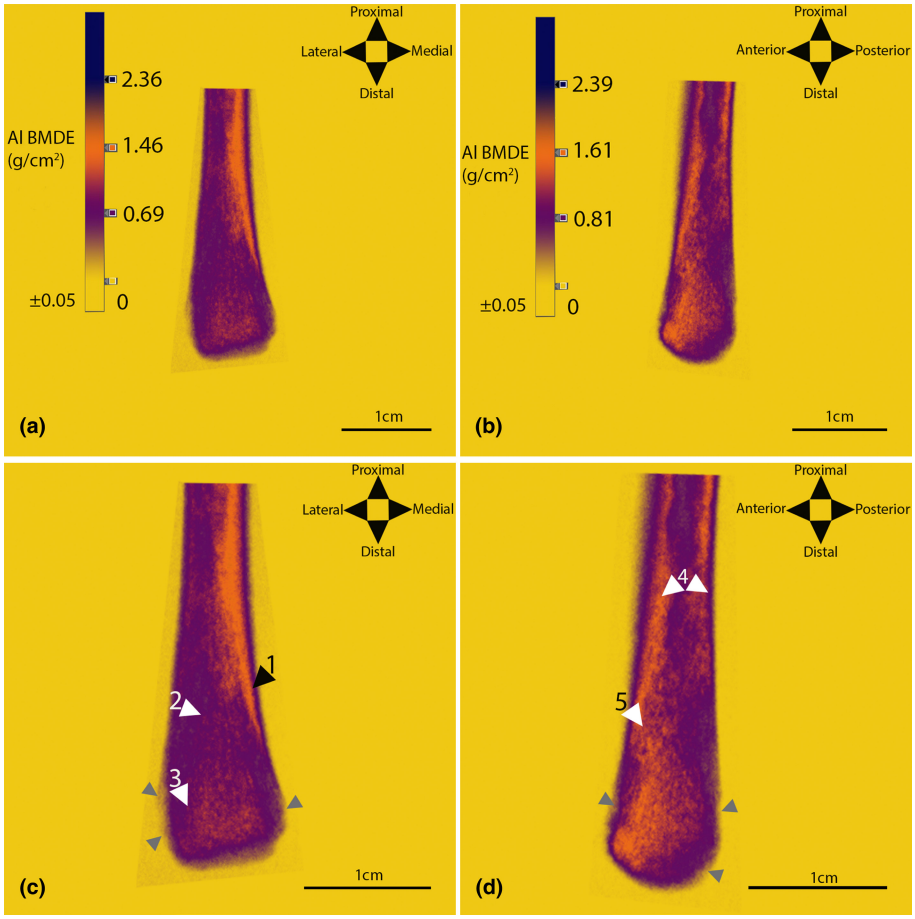

FIGURE 6 Annotated example of a colour gradient map of the right distal tibia from a Group 2 individual. (a, c) Anteroposterior view; (b, d) lateral view. Arrow descriptions are contained within Table 4.

TABLE 4 Radiographic features of a Group 2 tibia

Arrow	Feature
1	Medial margin of the diaphysis demonstrates medium AI BMDE depicted by orange extending down its surface
2	Struts radiating inferiorly from between the central and medial margin of the midshaft into the distal end of the tibia. This is typically demarcated by an orange colour indicating values of medium AI BMDE throughout
3	The orange demarcated by Arrow 2 increases in prevalence with increasing proximity to the distal end of the bone
4	Areas of medium AI BMDE illustrated by orange on the anterior and posterior margins of the midshaft
5	Orange triangular-shaped area of medium AI BMDE with the superior apex of the triangle extending from the anterior surface of the bone and into the distal end of the bone

Note: Arrows pertain to Figure 6.

Gardner et al., 1959). The invading nutrient artery supplies the tibia via the nutrient canal, typically located on the proximal posterior tibial surface. Recent literature, however, suggests that the blood supply to long bones is more complex than originally accepted, with hundreds of trans-cortical vessels traversing the cortical bone to the periosteum (Grüneboom et al., 2019), however, this did not appear observable via radiography. It may be that the spaces within the cortical bone containing these trans-cortical vessels are too small to visualise via this modality. Nevertheless, the vasculature of perinatal tibia appears less intrusive to the distal end of the bone, in comparison to the vascular system of the ilium, which may explain why the ilium appears to have a basic pattern similar to the adult form, but the tibia does not. It may be hypothesised that the vascular patterns of a bone are established prenatally and remain constant throughout life, thus explaining the shared observable patterns between adult and juvenile bones of complex vasculature. Further to this, the infant proximal femur and humerus have demonstrated similar trabecular structures to each other, which diverged only after the onset of the bipedal gait (Ryan et al., 2017). Therefore, this suggests that the radiographic pattern observed within the perinatal distal tibia perhaps presents a basic genetically pre-determined scaffold upon which locomotive forces can

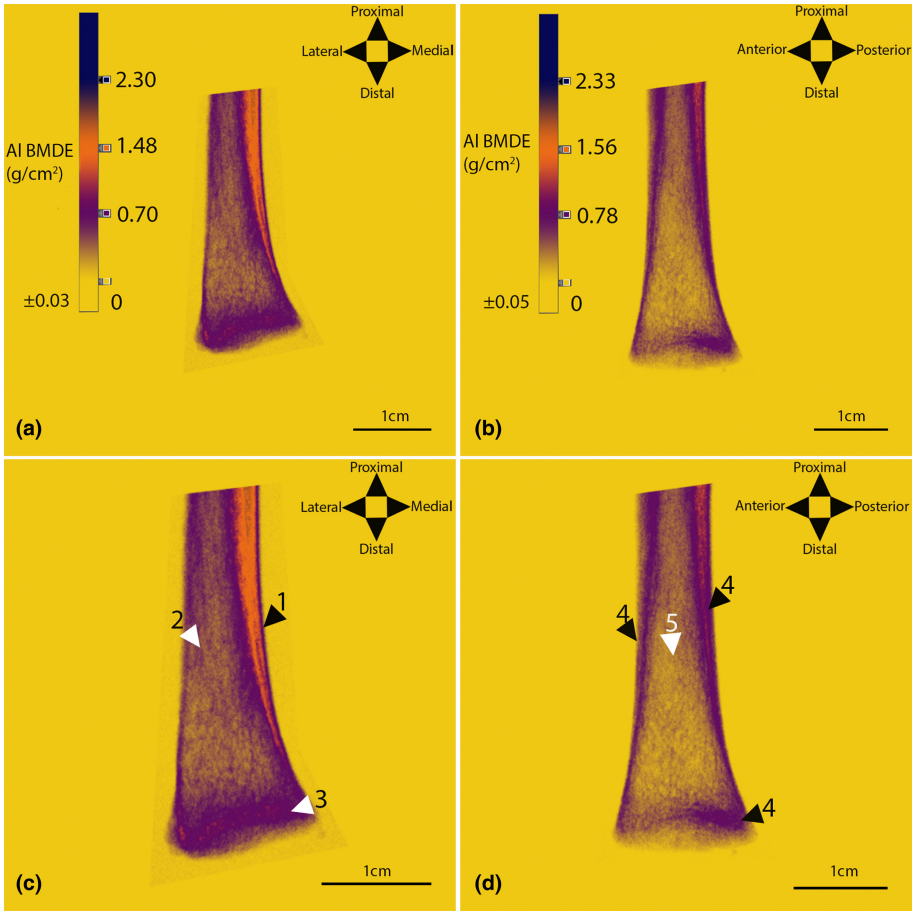

FIGURE 7 Annotated example of a colour gradient map of the right distal tibia from a Group 3 individual. (a, c) Anteroposterior view; (b, d) lateral view. Arrow descriptions are contained within Table 5.

TABLE 5 Radiographic features of a Group 3 tibia

Arrow	Feature
1	Orange area of medium AI BMDE extending down the medial margin of the tibia
2	Triangular radiolucency illustrated by the observable yellow background through the violet mottling throughout most of the distal portion of the bone indicating low AI BMDE
3	Distal-most aspect of the tibia exhibiting violet and an orange arched-shaped area indicating low-medium AI BMDE
4	Deep violet areas along the anterior, posterior and distal margins of the bone indicating low AI BMDE
5	The majority of the bone appears radiolucent demonstrated by yellow background appearing through the violet colouration indicating low AI BMDE

Note: Arrows pertain to Figure 7.

subsequently act at the onset of the bipedal gait, resulting in the more complex radiographic patterns observed after 2 years of age.

4.3 | Regression

Tibiae assigned to Group 3 (birth–2 years) appeared radiographically distinct from the rest of the tibial sample due to their radiolucency. The decreased radiopacity within the distal tibia indicates a decrease in AI BMDE in comparison to perinatal specimens. This decrease in radiodensity has also been observed previously within the developing ischium between 5 months and 2 years of age (Maclean, 2017) and within the scapula between 4 months and 5 years of age (O'Malley, 2013). Additionally, at approximately 6 months of age, a decrease in BV/TV has been observed in the femur (Milovanovic et al., 2017; Ryan et al., 2017; Ryan & Krovitz, 2006), proximal tibia (Gosman & Ketcham, 2009), calcaneus (Saers et al., 2019), humerus (Ryan et al., 2017), vertebrae (Acquaah et al., 2015) and ischium (Maclean, 2017). This period of decreasing BV/TV has been labelled as 'constructive regression' by Acquaah et al. (2015) and Maclean (2017).

Ryan and Krovitz (2006) suggest that the decrease in BV/TV at approximately 6 months in the developing proximal femur may be a

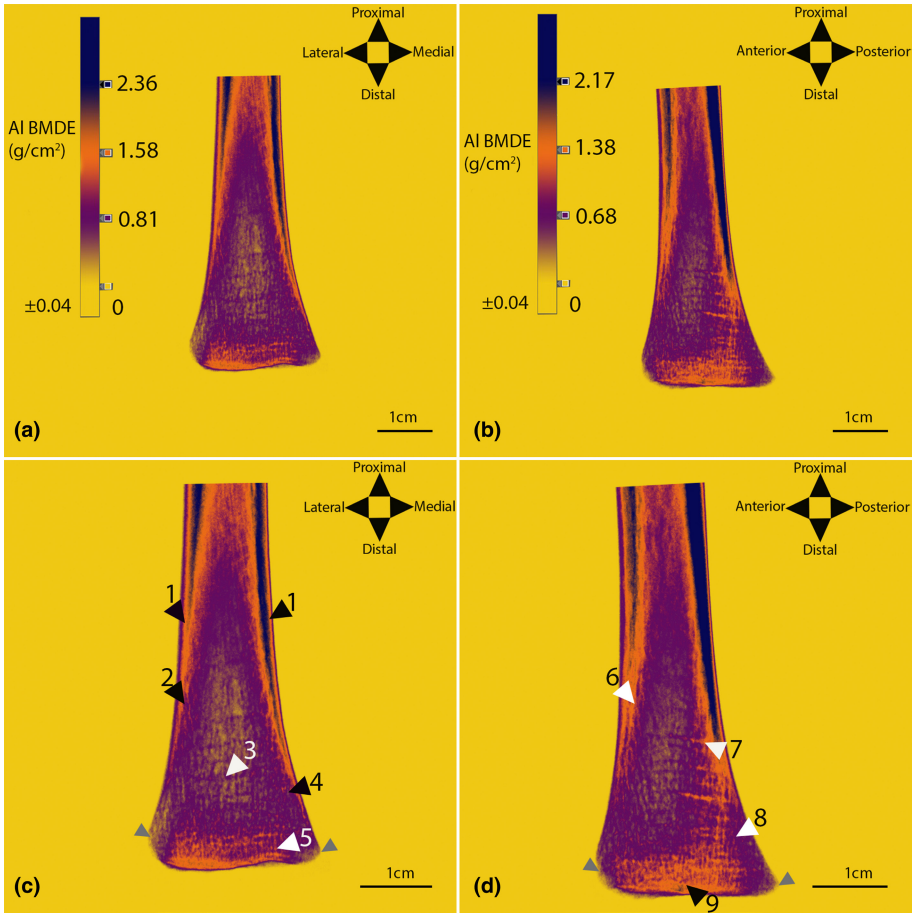

FIGURE 8 Annotated example of a colour gradient map of the right distal tibia from a Group 4 individual. (a, c) Anteroposterior view; (b, d) lateral view. Arrow descriptions are contained within Table 6.

TABLE 6 Radiographic features of a Group 4 tibia

Arrow	Feature
1	Medium to high AI BMDE exhibited on the medial and lateral margins of the bone towards the midshaft illustrated by an orange and blue colouration
2	Orange rays of medium AI BMDE extending infero-medially from the lateral margin of the bone. These rays appear violet distally
3	Transverse lines of violet travelling across the distal portion of the tibia. These appear consistent with Harris lines
4	Linear struts of violet and orange extending inferiorly towards the middle of the distal surface of the bone from the medial margin of the distal tibia
5	Mesh-like network of orange observed
6	Orange rays branching from the anterior surface of the bone. These orange struts extend infero-posteriorly towards the distal surface, becoming violet as they travel distally
7	Transverse lines travelling across the bone which appear orange towards the posterior aspect of the bone and become violet towards the anterior surface. These are consistent with Harris lines
8	Orange linear struts extending infero-anteriorly from the posterior surface of the bone towards the distal surface
9	Area of orange indicating medium AI BMDE on the distal surface of the bone which appears as a mesh-like network more superiorly and becomes denser with proximity to the distal margin of the bone

Note: Arrows pertain to Figure 8.

result of the remodelling process of the primary bone. The remodelling process is thought to reorganise the trabecular architecture at this stage to accommodate the development of the motor milestones such as the acquisition of crawling and walking. However, this decrease in BV/TV has also been hypothesised to be due to the lack of biomechanical activity at this stage of development which results in bone resorption following the Mechanostat hypothesis (Saers et al., 2019). This biomechanical influence may also account

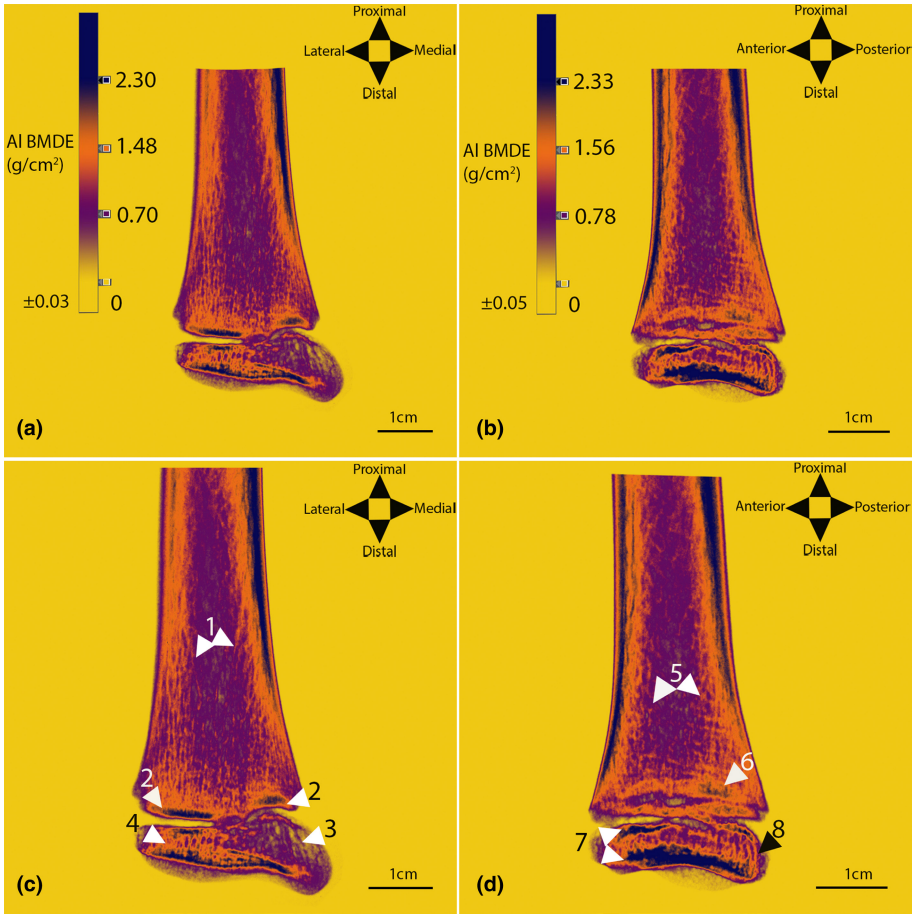

FIGURE 9 Annotated example of a colour gradient map of the right distal tibia from a Group 5 individual. (a, c) Anteroposterior view; (b, d) lateral view. Arrow descriptions are contained within Table 7.

TABLE 7 Radiographic features of a Group 5 tibia

Arrow	Feature
1	Orange struts of medium AI BMDE branching from the medial and lateral margins of the bone towards to the distal end of the bone
2	Areas of blue indicating high AI BMDE on the distal margin of the metaphysis
3	Violet struts of low AI BMDE fanning out from the superior surface of the developing medial malleolus within an area of radiolucency demonstrated by the visible yellow background
4	Thick linear orange rays between the superior and inferior margins of the lateral surface of the distal epiphysis which are blue depicting high AI BMDE
5	Trajectory of orange extending antero-inferiorly from the posterior surface of the tibia and postero-inferiorly from the anterior surface
6	Slight arched area of orange within the distal end of the bone that becomes blue posteriorly indicating an increase in AI BMDE
7	Blue areas of high AI BMDE along the superior and inferior portions of the distal epiphysis
8	Orange linear trajectory observed travelling between the superior and inferior portions of the distal epiphysis

Note: Arrows pertain to Figure 9.

for the decrease in radiodensity observed within the distal tibia between 0 and 2 years. The radiolucency of the distal tibia at this stage limits radiographic detail, however, the internal organisation of the distal tibia in specimens over 2 years of age, in comparison to perinatal specimens demonstrate an increase in complexity. Therefore, this period of radiolucency within the tibia may be a transitional stage where the architecture of the bone adjusts to the developing locomotive forces. This coincides with the period of high intra-individual variation in DA observed within the distal tibia, hypothesised to be related the instability associated with

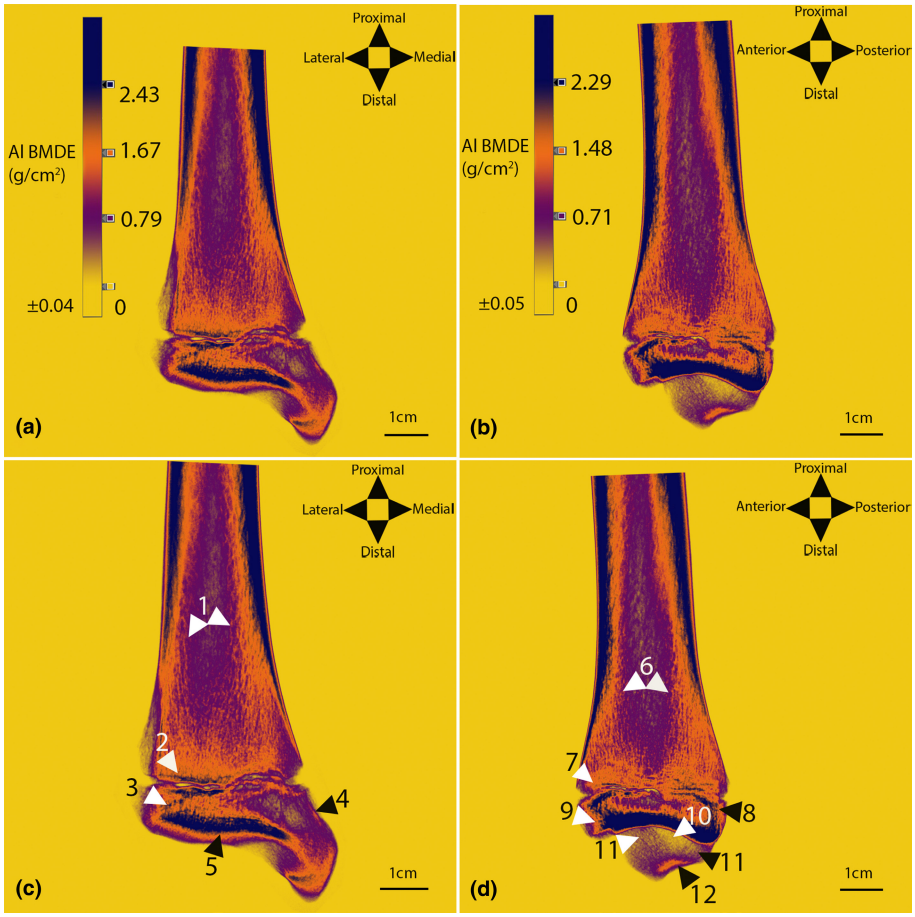

FIGURE 10 Annotated example of a colour gradient map of the right distal tibia from a Group 6 individual. (a, c) Anteroposterior view; (b, d) lateral view. Arrow descriptions are contained within Table 8.

TABLE 8 Radiographic features of a Group 6 tibia

Arrow	Feature
1	Orange struts of medium AI BMDE extending distally from both the medial and lateral aspects of the tibia
2	Thin line of blue illustrating an area of high AI BMDE among solid orange indicating medium AI BMDE along the distal surface of the diaphysis
3	Orange and blue struts travelling vertically between the superior and inferior aspects of the distal epiphysis
4	Triangular violet-coloured area within the superior portion of the medial malleolus with fine linear striations of violet and orange fanning from the superior aspect of the distal epiphysis
5	Blue area of high AI BMDE parallel to the talar facet
6	Orange trajectory travelling inferiorly from the anterior and posterior margins of the tibia
7	Area of dense orange along the distal surface of the diaphysis
8	Vertical trajectory between the superior and inferior distal epiphysis with high AI BMDE struts demarcated by blue on the anterior and posterior extremities of the epiphysis
9	Area of high AI BMDE depicted by solid blue extending throughout the inferior portion of the distal epiphysis
10	Triangular radiolucency within the centre of the medial malleolus
11	Fine linear violet struts extending inferiorly from the superior aspect of both the anterior and posterior colliculi towards intercollicular groove
12	Arched, orange-coloured area within the intercollicular groove indicating medium AI BMDE

Note: Arrows pertain to Figure 10.

learning to walk (Raichlen et al., 2015). If the radiolucency associated with Group 3 is attributed to this resorption hypothesis due to disuse, it questions whether there is a transition from genetic and vascular control associated with Groups 1 and 2, to biomechanical control for Group 3. This is in consensus with the hypothesis that genetic influences control intrauterine skeletal mass increase, followed by epigenetic and extragenetic influences, in the form of biomechanical forces, becoming more important after birth

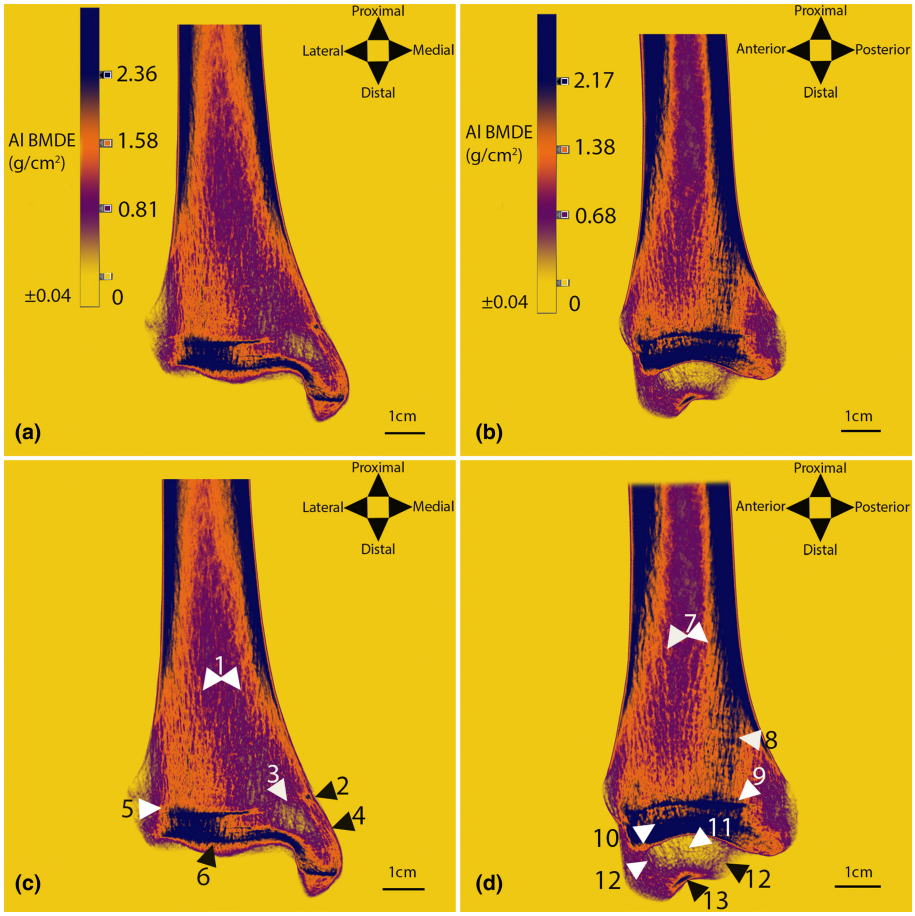

FIGURE 11 Annotated example of a colour gradient map of the right distal tibia from a Group 6 individual. (a, c) Anteroposterior view; (b, d) lateral view. Arrow descriptions are contained within Table 9.

when locomotion and muscle contractions become more dominant (Lanyon & Skerry, 2001; Skedros et al., 2004, 2007; Turner, 1998).

Factors beyond locomotive forces may also influence this radiolucency. Bone has multiple functions aside from its mechanical functions (Ruff et al., 2006; Turner, 2001). These additional functions include physiological demands such as the maintenance of blood calcium levels (Turner, 2001). In infants, calcium is typically acquired through breast milk, and therefore weaning and the transition to solid foods from approximately 6 months of age, may have an impact on calcium levels (Moore et al., 2014). Thus, the remodelling hypothesised to be driven by the onset of the locomotion (Ryan & Krovitz, 2006), may be also attributed to the need to liberate calcium from the skeleton to counteract the decrease in dietary calcium (Maclean, 2017). However, weaning at 6 months is more common in certain modern populations, and may not be applicable to archaeological specimens, such as the Scheuer collection, therefore other factors resulting in regression should also be considered.

Further to this, the influence of growth must also be noted. Three major phases of growth can be described within the skeleton; an initially rapid phase between birth and 2–3 years of age, a second phase after 3 years when growth slows until the final phase, the adolescent growth spurt (Lejarraga, 2012). Therefore, between 0 and 3 years, the skeleton exhibits substantial growth which also requires elevated modelling and remodelling activities. Combined with the decreased dietary calcium levels due to weaning (Moore et al., 2014), this may intensify demands to liberate calcium from the skeleton resulting in radiolucency within the skeleton at this stage (Maclean, 2017). This period of regression is likely due to a combination of factors including locomotive forces, weaning and growth resulting in a stage of development which is extremely demanding.

4.4 | Refinement

In comparison to tibiae ranging from 0 to 2 years during the period of 'regression', the radiodensity of the distal tibia increases after 2 years of age, associated with AI BMDE. This is in agreement with the increased BV/TV observed previously within the femur, vertebral column, proximal tibia and calcaneus (Acquaah et al., 2015; Gosman & Ketcham, 2009; Milovanovic et al., 2017; Ryan et al., 2017; Ryan & Krovitz, 2006; Saers et al., 2019). This has also been observed radiographically within the ischium between 1 and 3 years (Maclean, 2017), and within the scapula after 3 years of age (O'Malley, 2013).

After 2 years of age, the tibia exhibited trajectories that progressively developed into patterns consistent with adult trabecular

TABLE 9 Radiographic features of a Group 7 tibia

Arrow	Feature
1	Trajectory of orange extending distally from the medial and lateral margins of the bone. On the medial portion, these become violet coloured with proximity to the distal surface of the bone
2	Orange extending down the medial margin of the distal diaphysis and into the medial malleolus. Area of high AI BMDE, illustrated by blue, remains on the medial epiphyseal line
3	Radiolucency, indicated by the observable yellow background, within the superior aspect of the medial malleolus
4	Orange striations along the medial margin of the medial malleolus
5	Epiphyseal line remaining between the diaphysis and fused epiphysis which ranges from violet, orange and blue in colour
6	Struts travelling between the inferior and superior portion of the fused distal epiphysis which is of high AI BMDE values towards the lateral aspect of the bone
7	Orange trajectory extending inferiorly from the anterior and posterior surfaces of the diaphysis
8	Blue trajectory of high AI BMDE extending antero-inferiorly from the posterior surface of the bone
9	Blue line of high AI BMDE equivalents along the epiphyseal line
10	Blue area of high AI BMDE superior to the distal articular surface
11	Radiolucency of the centre of the medial malleolus demonstrated by the observable yellow background. Fine violet struts can be observed within this area
12	Fine linear violet struts extending inferiorly from the superior aspect of both the anterior and posterior colliculi towards intercollicular groove
13	Arched, blue-coloured area within the intercollicular groove

Note: Arrows pertain to Figure 11.

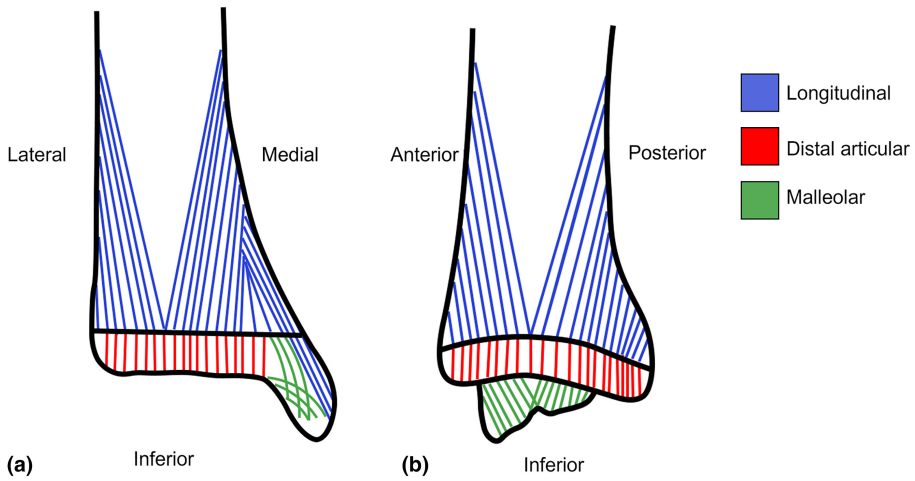

FIGURE 12 Proposed trajectories within the right tibia. (a) Anterior view; (b) medial view.

organisation. This is consistent with the period of 'constructive refinement' coined by Acquaah et al. (2015) which is associated with an increase in BV/TV and a development of structural heterogeneity within skeletal elements related to their functional requirements. These functional requirements are predominately associated with the acquisition of motor milestones and the bipedal gait. The ability to sit upright occurs at approximately 6 months of age, while crawling on hands and feet normally begins around 8 months, with cruising following at 9 months of age (Keen, 1993). The onset of walking occurs at approximately 12–14.5 months of age (Keen, 1993; Størvold et al., 2013). The bipedal gait of an infant is not a smaller version of the adult gait but has its own unique developing biomechanical patterns (Rose & Gamble, 1994). Early walking is typically described as having a wide stance combined with flexion of both the knee and hip (Cowgill et al., 2010; Hallemans et al., 2005; Johnston et al., 2014; Sutherland, 1997; Sutherland et al., 1988). During this stage, the plantar fat pad defends the foot against overloading, dispersing the plantar pressure throughout the foot (Bosch et al., 2007). After 18 months of age, there is a shift in load from the midfoot to the heel and forefoot as the longitudinal arch of the foot develops resulting in plantarflexion during the gait cycle (Bertsch et al., 2004; Bosch et al., 2007; Sutherland et al., 1988). There is debate regarding the timing of maturation of the bipedal gait, however, it appears to occur between 4 and 8 years of age (Saers et al., 2019; Sutherland, 1997).

Despite Raichlen et al. (2015) observing high inter-individual variation in the distal tibia between 0.5 and 4.9 years, that was

attributed to the instability associated with learning to walk, distinct differences in radiographic patterns between individuals from Group 4 (2–10 years) were not observed. This may be associated with the small sample size of Group 4 ($n = 9$ individuals). Nevertheless, it should also be considered that DA is a quantifiable measure conducted using μCT, and that changes in DA therefore may not be observable using radiography. The subsequent μCT analysis of this sample may provide more detailed insight into variation between specimens of similar age-at-deaths. Additionally, no distinct shifts in the organisation of the tibia were observable around 18 months of age during the development of the longitudinal arch of the foot, resulting in the production of ankle plantarflexion during walking. A larger sample size of specimens aged around 1–3 years may provide greater clarity into any changes associated with the development of the longitudinal arch, as will a subsequent μCT study.

While several trabecular trajectories are described within the literature examining the adult tibia, they lack standardised naming. Therefore, based on the observations within this study of the late adolescent tibia combined with the adult literature, the following trajectories are proposed to develop within the juvenile tibia: longitudinal, distal articular and malleolar trajectories (Figure 12).

After 2 years of age, trajectories were observed descending from the medial, lateral, anterior and posterior boundaries of the diaphysis inferiorly and obliquely towards the centre of the distal surface of the bone. These are proposed as the 'longitudinal' trajectories (blue lines, Figure 12). The distal end of the bone consistently exhibited an area of medium to high AI BMDE where these trajectories appeared to converge. The trajectories observed within the distal diaphysis are consistent with the trajectories observed by Takechi et al. (1982) in the adult tibia. These are believed to facilitate the transmission of compressive forces from the body down through the tibia and into the foot via the talus (Takechi et al., 1982). They are therefore associated with weight-bearing in a passive stance and during the bipedal stance. Thus, the appearance of these trajectories at 2 years of age is consistent with the acquisition of the bipedal gait.

The distal epiphysis was observed in specimens in Group 5 onwards (7–9 years). A trajectory, named the distal articular trajectory (red lines, Figure 12) was observed superior to the roof of the talar facet, extending vertically between the superior and inferior portions of the epiphysis. The distal articular surface consistently exhibited blue indicating high AI BMDE. The presence of thick vertically aligned trabeculae has been observed within the distal articular surface of the adult tibia (Takechi et al., 1982), in addition to being associated with high BV/TV values (Tsegai et al., 2017). These trabeculae in the adult distal articular surface of the tibia are believed to be adapted to facilitate the transmission of high compressive bodyweight forces through to the talus (Procter & Paul, 1982; Stauffer et al., 1977).

In the medial malleolus in specimens within Group 6 and 7 (10 years–late adolescence), malleolar trajectories were observed. In the oldest of specimens these trajectories appeared to curve both transversely and vertically (malleolar trajectories, green lines, Figure 12). In the adult tibia, the trabeculae nearest the talar facet within the malleolus have been observed to be transversely orientated, while the medial trabeculae were organised vertically (Figure 1) (Takechi et al., 1982; Tillmann et al., 1985). Additionally, transversely orientated trabeculae were described in the 'shoulder' of the medial malleolus (Takechi et al., 1982; Tillmann et al., 1985). These trabeculae in the adult medial malleolus are proposed to be vertically aligned to compressive forces and to facilitate tensile forces in the malleolus caused by collateral ankle ligaments (Tillmann et al., 1985). Thus, from 2 years of age, the organisation of the juvenile tibia begins to develop in association with its functional requirements within the ankle joint to facilitate the transmission of forces during passive standing and the bipedal gait from the body, cumulating in an adult-like morphology by 10 years of age.

A novel method combining radiographic absorptiometry and colour gradient maps was introduced to facilitate the observation of the internal arrangement of the distal tibia from the prenatal period through to late adolescence. This novel method may be of clinical and forensic use; for example, in the identification of trabecular disruption experienced during juvenile classic metaphyseal lesions, which are typically difficult to identify under standard radiographic analysis (Love et al., 2011). Reporting AI BMDE with reference to an aluminium step wedge provides comparable, standardised results, in contrast to reporting bone intensities. Nevertheless, radiographic absorptiometry does not overcome the issues with tissue superimposition experienced within x-rays, and therefore any AI BMDE value reported will be influenced by this. Due to this AI BMDEs were used more as a guide for interpretation rather than tool for definitive comparisons, and no extensive quantification or analysis of these values were conducted. As such, while reporting relative bone density as AI BMDE is an improvement upon previous studies recording arbitrary bone intensities, the results need to be validated through a μCT examination. The superimposition of tissues within a radiographic image also meant that it was not possible to determine whether a pattern observed within a specimen was due to its trabecular or its cortical organisation. As such, patterns were not identified as trabeculae or as the cortex, but instead referred to in terms such as 'trajectory', 'strut', 'ray' or 'pattern'. These 'patterns' were then subsequently compared to trabecular trajectories previously described within the adult distal tibia, to postulate their function.

Interobserver agreement of placement of the colour maps into developmental groups was assessed as good to very good, while intraobserver agreement was very good. This suggests that this approach to radiographic analysis can reliably identify developmental patterns.

This study was limited by small sample sizes representing different age groups. In particular, foetal specimens were poorly represented. As such, any observations from these younger specimens are preliminary and must be confirmed following analysis on a larger sample. In addition to this, the lack of documentation for the Scheuer Collection limits results. While the ages of some specimens were documented, the age-at-death for most of the sample was estimated. Therefore, the ages provided for each developmental period

identified (foetal, perinatal, regression and refinement) should be interpreted with caution and seen as approximate timings for developmental changes, not definitive timings. Additionally, information such as cause of death, pathology, ancestry, sex and socio-economic status was unknown for several specimens. Given that cause of death and pathology is unknown for several of the individuals within the Scheuer Collection, it is not possible to evaluate how this may affect skeletal development and thus the results of this study. The Scheuer collection is also predominately an archaeological population, as is the majority of research examining juvenile development, therefore the applicability of the results of this study upon a modern population is unknown.

5 | CONCLUSION

This radiographic study aimed to identify preliminary patterns and phases during the development of the distal tibia. A novel approach was adopted for the radiographic analysis which combined radiographic absorptiometry with colour gradient maps. Distinct developmental phases were observed: the foetal, perinatal, regressive and refinement period. The foetal tibia demonstrated limited radiographic features, however, appeared consistent with reported ossification patterns. The perinatal tibia (birth–6 months) did not share a rudimentary structural pattern similar to the architecture observed within the late adolescent tibia. In group 3 individuals, between birth and 2 years of age, the tibia exhibited a period of regression where radiodensity decreased in comparison to the perinatal tibia. This period of regression is hypothesised to be due to a combination of factors including locomotive forces, weaning and rapid growth resulting in a stage of development which is extremely demanding. After 2 years of age, the distal tibia demonstrated refinement where radiographic trajectories progressively developed into patterns consistent with adult trabecular organisation which are strongly linked to the forces associated by the bipedal gait. The development of such trajectories from 2 years of age occurs after the onset of walking at approximately 12–14.5 months of age, suggesting a strong influence of locomotive forces on the development of the distal tibia and talus.

AUTHOR CONTRIBUTIONS

RR was involved in study design, data acquisition and collection, data interpretation, manuscript design, preparation, revision and review. CC and CD were involved in study design, data interpretation, manuscript revision and review.

ACKNOWLEDGEMENTS

This work was supported by the University of Dundee Greenhouse Scholarship. Many thanks to Observer 2 for their participation in the interobserver agreement study. Thanks also to Ms. Claire Cunningham and Mr Tyler Halliwell for their technical radiographic assistance. We are extremely grateful for the reviewers for their invaluable recommendations.

CONFLICT OF INTEREST

None.

DATA AVAILABILITY STATEMENT

Data available on request from authors. The data that support the findings of this study are available from the corresponding author upon reasonable request.

ORCID

Rebecca A. G. Reid https://orcid.org/0000-0002-1325-1963
Catriona Davies https://orcid.org/0000-0002-9569-701X
Craig Cunningham https://orcid.org/0000-0003-2730-762X

REFERENCES

Abel, R. & Macho, G.A. (2011) Ontogenetic changes in the internal and external morphology of the ilium in modern humans. *Journal of Anatomy*, 218(3), 324–335.

Acquaah, F., Robson Brown, K.A., Ahmed, F., Jeffery, N. & Abel, R.L. (2015) Early trabecular development in human vertebrae: overproduction, constructive regression, and refinement. *Frontiers in Endocrinology*, 6(67), 1–9.

Barak, M.M., Lieberman, D.E. & Hublin, J.-J. (2011) A Wolff in sheep's clothing: trabecular bone adaptation in response to changes in joint loading orientation. *Bone*, 49(6), 1141–1151.

Baumgart, M., Wiśniewski, M., Grzonkowska, M., Badura, M., Szpinda, M. & Pawlak-Osińska, K. (2019) Three-dimensional growth of tibial shaft ossification in the human fetus: a digital-image and statistical analysis. *Surgical and Radiologic Anatomy*, 41(1), 87–95.

Beresheim, A.C., Pfeiffer, S. & Grynpas, M. (2020) Ontogenetic changes to bone microstructure in an archaeologically derived sample of human ribs. *Journal of Anatomy*, 236(3), 448–462.

Bertsch, C., Unger, H., Winkelmann, W. & Rosenbaum, D. (2004) Evaluation of early walking patterns from plantar pressure distribution measurements. First year results of 42 children. *Gait and Posture*, 19(3), 235–242.

Bosch, K., Gerss, J. & Rosenbaum, D. (2007) Preliminary normative values for foot loading parameters of the developing child. *Gait and Posture*, 26(2), 238–247.

Bowen, A.J., Burd, M.A., Craig, J.J. & Craig, M. (2013) Radiographic calibration for analysis of bone mineral density of the equine third metacarpal bone. *Journal of Equine Veterinary Science*, 33(12), 1131–1135.

Burrows, M., Liu, D., Moore, S. & McKay, H. (2010) Bone microstructure at the distal tibia provides a strength advantage to males in late puberty: an HR-pQCT study. *Journal of Bone and Mineral Research*, 25(6), 1423–1432.

Byers, S., Moore, A.J., Byard, R.W. & Fazzalari, N.L. (2000) Quantitative histomorphometric analysis of the human growth plate from birth to adolescence. *Bone*, 27(4), 495–501.

Cicchetti, D.V. & Allison, T. (1971) A new procedure for assessing reliability of scoring EEG sleep recordings. *American Journal of EEG Technology*, 11, 101–109.

Colombo, A., Stephens, N.B., Tsegai, Z.J., Bettuzzi, M., Morigi, M.P., Belcastro, M.G. et al. (2019) Trabecular analysis of the distal radial metaphysis during the acquisition of crawling and bipedal walking in childhood: a preliminary study. *Bulletins et Mémoires de la Société d'Anthropologie de Paris*, 31(1–2), 43–51.

Cowgill, L.W., Warrener, A., Pontzer, H. & Ocobock, C. (2010) Waddling and toddling: the biomechanical effects of an immature gait. *American Journal of Physical Anthropology*, 143(1), 52–61.

Cunningham, C.A. & Black, S.M. (2009a) Development of the fetal ilium—Challenging concepts of bipedality. *Journal of Anatomy*, 214(1), 91–99.

Cunningham, C.A. & Black, S.M. (2009b) Anticipating bipedalism: trabecular organization in the newborn ilium. *Journal of Anatomy*, 214(6), 817–829.

Cunningham, C.A. & Black, S.M. (2009c) Iliac cortical thickness in the neonate - the gradient effect. *Journal of Anatomy*, 215(3), 364–370.

Cunningham, C.A. & Black, S.M. (2010) The neonatal ilium-metaphyseal drivers and vascular passengers. *The Anatomical Record: Advances in Integrative Anatomy and Evolutionary Biology*, 293(8), 1297–1309.

Cunningham, C.A. & Black, S.M. (2013) The vascular collar of the ilium-Three-dimensional evaluation of the dominant nutrient foramen: the iliac nutrient collar. *Clinical Anatomy*, 26(4), 502–508.

Cunningham, C., Scheuer, L. & Black, S. (2016) Chapter 12—The lower limb. In: Cunningham, I.C., Scheuer, L. & Black, S. (Eds.) *Developmental juvenile osteology*, 2nd edition. London: Academic Press, pp. 385–472.

Currey, J. (1984) *The mechanical adaptations of bones*. New Jersey: Princeton University Press.

Ding, M., Danielsen, C.C., Hvid, I. & Overgaard, S. (2012) Three-dimensional microarchitecture of adolescent cancellous bone. *Bone*, 51(5), 953–960.

Djuric, M., Milovanovic, P., Djonic, D., Minic, A. & Hahn, M. (2012) Morphological characteristics of the developing proximal femur: A biomechanical perspective. *Srpski Arhiv za Celokupno Lekarstvo*, 140(11–12), 738–745.

Du, J., Brooke-Wavell, K., Paggiosi, M.A., Hartley, C., Walsh, J.S., Silberschmidt, V.V. et al. (2019) Characterising variability and regional correlations of microstructure and mechanical competence of human tibial trabecular bone: an in-vivo HR-pQCT study. *Bone*, 121, 139–148.

Fazzalari, N.L., Moore, A.J., Byers, S. & Byard, R.W. (1997) Quantitative analysis of trabecular morphogenesis in the human costochondral junction during the postnatal period in normal subjects. *The Anatomical Record*, 248(1), 1–12.

Frost, H.M. (1998) Changing concepts in skeletal physiology: Wolff's Law, the Mechanostat, and the "Utah Paradigm". *American Journal of Human Biology*, 10(5), 599–605.

Frost, H.M. (2003) Bone's mechanostat: A 2003 update. *The Anatomical Record Part A: Discoveries in Molecular, Cellular, and Evolutionary Biology*, 275A(2), 1081–1101.

Gardner, E., Gray, D.J. & O'Rahilly, R. (1959) The prenatal development of the skeleton and joints of the human foot. *The Journal of Bone and Joint Surgery American*, 41-A(5), 847–876.

Gasser, K.M., Mueller, C., Zwahlen, M., Kaufmann, M., Fuchs, G., Perrelet, R. et al. (2005) Osteoporosis case finding in the general practice: Phalangeal radiographic absorptiometry with and without risk factors for osteoporosis to select postmenopausal women eligible for lumbar spine and hip densitometry. *Osteoporosis International*, 16(11), 1353–1362.

Glorieux, F.H., Travers, R., Taylor, A., Bowen, J.R., Rauch, F., Norman, M. et al. (2000) Normative data for iliac bone histomorphometry in growing children. *Bone*, 26(2), 103–109.

Goodchild, S. (2019). *A qualitative and quantitative analysis of the developing lumbar vertebral column*. PhD Thesis, University of Dundee, Dundee. Available at: https://discovery.dundee.ac.uk/en/studentTheses/a-qualitative-and-quantitative-analysis-of-the-developinGg-human-l

Goliath, J.R., Gosman, J., Stout, S. & Ryan, T. (2022) Ontogenetic patterning of human subchondral bone microarchitecture in the proximal tibia. *Biology*, 11(7), 1002.

Gosman, J.H. & Ketcham, R.A. (2009) Patterns in ontogeny of human trabecular bone from SunWatch village in the Prehistoric Ohio valley: general features of microarchitectural change. *American Journal of Physical Anthropology*, 138(3), 318–332.

Grüneboom, A., Hawwari, I., Weidner, D., Culemann, S., Müller, S., Henneberg, S. et al. (2019) A network of trans-cortical capillaries as mainstay for blood circulation in long bones. *Nature Metabolism*, 1(2), 236–250.

Hallemans, A., De Clercq, D., Otten, B. & Aerts, P. (2005) 3D joint dynamics of walking in toddlers: a cross-sectional study spanning the first rapid development phase of walking. *Gait and Posture*, 22(2), 107–118.

Hirvasniemi, J., Niinimäki, J., Thevenot, J. & Saarakkala, S. (2019) Bone density and texture from minimally post-processed knee radiographs in subjects with knee osteoarthritis. *Annals of Biomedical Engineering*, 47(5), 1181–1190.

Ilić, D., Stojanović, L., Antonijević, D., Milutinović-Smiljanić, S., Savić-Stanković, T. & Milosavljević, Ž. (2020) Measuring of mandible bone density in dogs using /digital radiography/radiovisigraphy. *Acta Veterinaria*, 70(3), 285–295.

Johnston, L., Eastwood, D. & Jacobs, B. (2014) Variations in normal gait development. *Paediatrics and Child Health*, 24(5), 204–207.

Keen, M. (1993) Early Development and attainment of normal mature gait. *JPO: Journal of Prosthetics and Orthotics*, 5(2), 35–38.

Kneissel, M., Roschger, P., Steiner, W., Schamall, D., Kalchhauser, G., Boyde, A. et al. (1997) Cancellous bone structure in the growing and aging lumbar spine in a historic nubian population. *Calcified Tissue International*, 61(2), 95–100.

Landis, J.R. & Koch, G.G. (1977) The measurement of observer agreement for categorical data. *Biometrics*, 33(1), 159–174.

Lanyon, L. & Skerry, T. (2001) Postmenopausal osteoporosis as a failure of bone's adaptation to functional loading: a hypothesis. *Journal of Bone and Mineral Research*, 16(11), 1937–1947.

Lejarraga, H. (2012) Chapter 2 - Growth in infancy and childhood: a pediatric approach. In: Cameron, N. & Bogin, B. (Eds.) *Human growth and development*, 2nd edition. San Diego: Academic Press, pp. 23–56.

Love, J.C., Derrick, S.M. & Wiersema, J.M. (2011) *Skeletal atlas of child abuse*. New York: Humana Press.

Maclean, S. J. (2017). *A qualitative and quantitative analysis of the juvenile ischium*. PhD Thesis, University of Dundee, Dundee. Available at: https://discovery.dundee.ac.uk/en/studentTheses/a-qualitative-and-quantitative-analysis-of-the-juvenile-ischium.

Maclean, S.J., Black, S.M. & Cunningham, C.A. (2014) The developing juvenile ischium: macro-radiographic insights: the developing juvenile ischium. *Clinical Anatomy*, 27(6), 906–914.

Marsh, J.S. & Daigneault, J.P. (2000) Ankle injuries in the pediatric population. *Current Opinion in Pediatrics*, 12(1), 52–60.

Milovanovic, P., Djonic, D., Hahn, M., Amling, M., Busse, B. & Djuric, M. (2017) Region-dependent patterns of trabecular bone growth in the human proximal femur: a study of 3D bone microarchitecture from early postnatal to late childhood period. *American Journal of Physical Anthropology*, 164(2), 281–291.

Modlesky, C.M., Whitney, D.G., Carter, P.T., Allerton, B.M., Kirby, J.T. & Miller, F. (2014) The pattern of trabecular bone microarchitecture in the distal femur of typically developing children and its effect on processing of magnetic resonance images. *Bone*, 60, 1–7.

Moore, A.P., Milligan, P. & Goff, L.M. (2014) An online survey of knowledge of the weaning guidelines, advice from health visitors and other factors that influence weaning timing in UK mothers. *Maternal & Child Nutrition*, 10(3), 410–421.

Nackaerts, O., Jacobs, R., Horner, K., Zhao, F., Lindh, C., Karayianni, K. et al. (2007) Bone density measurements in intra-oral radiographs. *Clinical Oral Investigations*, 11(3), 225–229.

Nuzzo, S., Meneghini, C., Braillon, P., Bouvier, R., Mobilio, S. & Peyrin, F. (2003) Microarchitectural and physical changes during fetal growth in human vertebral bone. *Journal of Bone and Mineral Research*, 18(4), 760–768.

O'Malley, A. (2013). *A qualitative and quantitative investigation of the functional morphology of the juvenile scapula*. PhD Thesis, University of Dundee. Available at: https://discovery.dundee.ac.uk/en/studentTheses/a-qualitative-and-quantitative-investigation-of-the-functional-mo.

Osborne, D., Effmann, E., Broda, K. & Harrelson, J. (1980) The development of the upper end of the femur, with special reference to its internal architecture. *Radiology*, 137(1 Pt 1), 71–76.

Perchalski, B., Placke, A., Sukhdeo, S.M., Shaw, C.N., Gosman, J.H., Raichlen, D.A. et al. (2018) Asymmetry in the cortical and trabecular bone of the human humerus during development. *The Anatomical Record*, 301(6), 1012–1025.

Procter, P. & Paul, J.P. (1982) Ankle joint biomechanics. *Journal of Biomechanics*, 15(9), 627–634.

Raichlen, D.A., Gordon, A.D., Foster, A.D., Webber, J.T., Sukhdeo, S.M., Scott, R.S. et al. (2015) An ontogenetic framework linking locomotion and trabecular bone architecture with applications for reconstructing hominin life history. *Journal of Human Evolution*, 81, 1–12.

Reed, M.H. & Black, G.B. (2010) Fractures of the ankle. In: Medina, L.S., Applegate, K.E. & Blackmore, C.C. (Eds.) *Evidence-based imaging in pediatrics: optimizing imaging in pediatric patient care*. New York: Springer, pp. 329–336.

Reissis, D. & Abel, R.L. (2012) Development of fetal trabecular microarchitecture in the humerus and femur. *Journal of Anatomy*, 220(5), 496–503.

Roschger, P., Grabner, B.M., Rinnerthaler, S., Tesch, W., Kneissel, M., Berzlanovich, A. et al. (2001) Structural development of the mineralized tissue in the human L4 vertebral body. *Journal of Structural Biology*, 136(2), 126–136.

Rose, J. & Gamble, J.G. (1994) *Human walking*, 2nd edition. Baltimore: Lippincott Williams and Wilkins.

Ruff, C., Holt, B. & Trinkaus, E. (2006) Who's afraid of the big bad Wolff?: "Wolff's law" and bone functional adaptation. *American Journal of Physical Anthropology*, 129(4), 484–498.

Ruimerman, R., Hilbers, P., van Rietbergen, B. & Huiskes, R. (2005) A theoretical framework for strain-related trabecular bone maintenance and adaptation. *Journal of Biomechanics*, 38(4), 931–941.

Ryan, T.M. & Krovitz, G.E. (2006) Trabecular bone ontogeny in the human proximal femur. *Journal of Human Evolution*, 51(6), 591–602.

Ryan, T.M., Raichlen, D.A. & Gosman, J.H. (2017) Structural and mechanical changes in trabecular bone during early development in the human femur and humerus. In: Percival, C.J. & Richtsmeier, J.T. (Eds.) *Building bones: bone formation and development in anthropology*. Cambridge: Cambridge University Press, pp. 281–302.

Saers, J.P.P., Ryan, T.M. & Stock, J.T. (2019) Baby steps towards linking calcaneal trabecular bone ontogeny and the development of bipedal human gait. *Journal of Anatomy*, 236(3), 474–492.

Saers, J.P.P., Gordon, A.D., Ryan, T.M. & Stock, J.T. (2022) Growth and development of trabecular structure in the calcaneus of Japanese macaques (Macaca fuscata) reflects locomotor behavior, life history, and neuromuscular development. *Journal of Anatomy*, 241(1), 67–81.

Salle, B.L., Rauch, F., Travers, R., Bouvier, R. & Glorieux, F.H. (2002) Human fetal bone development: histomorphometric evaluation of the proximal femoral metaphysis. *Bone*, 30(6), 823–828.

Skedros, J.G., Hunt, K.J. & Bloebaum, R.D. (2004) Relationships of loading history and structural and material characteristics of bone: development of the mule deer calcaneus. *Journal of Morphology*, 259(3), 281–307.

Skedros, J.G., Sorenson, S.M., Hunt, K.J. & Holyoak, J.D. (2007) Ontogenetic structural and material variations in ovine calcanei: a model for interpreting bone adaptation. *The Anatomical Record*, 290(3), 284–300.

Soames, R.W. & Palastanga, N. (2019) Lower limb. In: Soames, R.W. & Palastanga, N. (Eds.) *Anatomy and human movement*, 7th edition. London: Elsevier, pp. 219–434.

Sode, M., Burghardt, A.J., Kazakia, G.J., Link, T.M. & Majumdar, S. (2010) Regional variations of gender-specific and age-related differences in trabecular bone structure of the distal radius and tibia. *Bone*, 46(6), 1652–1660.

Stauffer, R.N., Chao, E.Y. & Brewster, R.C. (1977) Force and motion analysis of the normal, diseased, and prosthetic ankle joint. *Clinical Orthopaedics and Related Research*, 127, 189–196.

Størvold, G.V., Aarethun, K. & Bratberg, G.H. (2013) Age for onset of walking and prewalking strategies. *Early Human Development*, 89(9), 655–659.

Sun, Y., De Dobbelaer, B., Nackaerts, O., Loubele, M., Yan, B., Suetens, P. et al. (2008) Development of a clinically applicable tool for bone density assessment. *International Journal of Computer Assisted Radiology and Surgery*, 4(2), 163.

Sutherland, D. (1997) The development of mature gait. *Gait & Posture*, 6(2), 163–170.

Sutherland, D.H., Olshen, R.A., Biden, E.N. & Wyatt, M.P. (1988) *The development of mature walking*. London: Mac Keith Press.

Takechi, H., Ito, S., Takada, T. & Nakayama, H. (1982) Trabecular architecture of the ankle joint. *Anatomia Clinica*, 4(3), 227–233.

Tillmann, B., Bartz, B. & Schleicher, A. (1985) Stress in the human ankle joint: a brief review. *Archives of Orthopaedic and Traumatic Surgery*, 103(6), 385–391.

Trouerbach, W.T. (1982), *Radiographic aluminum equivalent value of bone: the development of a registration method and some clinical applications*. PhD Thesis, University Medical Center Rotterdam. Available at: http://hdl.handle.net/1765/32131.

Tsegai, Z.J., Skinner, M.M., Gee, A.H., Pahr, D.H., Treece, G.M., Hublin, J.J. et al. (2017) Trabecular and cortical bone structure of the talus and distal tibia in Pan and Homo. *American Journal of Physical Anthropology*, 163(4), 784–805.

Turner, C.H. (1998) Three rules for bone adaptation to mechanical stimuli. *Bone*, 23(5), 399–407.

Turner, R.T. (2001) Skeletal adaptation to external loads optimizes mechanical properties: fact or fiction. *Current Opinion in Orthopaedics*, 12(5), 384–388.

van Rijn, R.R., Lequin, M.H., van Leeuwen, W.J., Hop, W.C.J. & van Kuijk, C. (2000) Radiographic absorptiometry of the middle phalanx (Digit II) in a caucasian pediatric population: normative data. *Osteoporosis International*, 11(3), 240–247.

White, J.R., Wilsman, N.J., Leiferman, E.M. & Noonan, K.J. (2008) Histomorphometric analysis of an adolescent distal tibial physis prior to growth plate closure. *Journal of Children's Orthopaedics*, 2(4), 315–319.

Yusof, N.A. (2013). *The development and anatomy of the sacrum in relation to the ilium and the sacroiliac joint*. PhD Thesis, University of Dundee, Dundee. Available at: https://discovery.dundee.ac.uk/en/studentTheses/the-development-and-anatomy-of-the-sacrum-in-relation-to-the-iliu.

How to cite this article: Reid, R.A.G., Davies, C. & Cunningham, C. (2023) The developing juvenile distal tibia: Radiographic identification of distinct ontogenetic phases and structural trajectories. *Journal of Anatomy*, 242, 191–212. Available from: https://doi.org/10.1111/joa.13778